IMPACT OF SUBGRID-SCALE PARAMETERIZATIONS ON MONTHLY FORECASTS

by K. Miyakoda and J. Sirutis
Geophysical Fluid Dynamics Laboratory/NOAA
Princeton, New Jersey 08542

Summary: The effect of the subgrid-scale processes on the simulation of general circulation and gross weather were studied by incorporating various physics into a global finite difference model and carrying out 30-day integrations for three winter, one spring and one summer cases. Three models with different sets of parameterization schemes were: the first reference model, which uses the GFDL 1965 version of physics; the second model, which includes advanced boundary layer physics and turbulence closure scheme, excluding the dry convective adjustment; and the third model, which uses the Arakawa-Schubert cumulus parameterization. The impact of these processes on about 10 day integration was subtle and yet significant. The second and the third models were noticeably better than the first model in the performance of 10 day forecast. The differences of the three models in 30 day forecasts were appreciable in all cases treated. The third model produced the best prediction results consistently for winter and spring cases. The distribution of tropical rainfall is spatially smooth, which appears to be realistic, and less gravity waves than other models are generated. The impact of cumulus parameterization is significant especially in the tropics. The effect of the elaborate subgrid-scale schemes in the second model is also appreciable in the tropical region. The subject treated in this paper is relevant to the issue of equatorial heating and its teleconnection with the extratropical circulation. Perhaps the most pronounced impact in the second and the third models is that large amplitude meandering westerlies in the middle and high latitudes were produced, implying that the simulation of blocking ridges has been improved.

1. INTRODUCTION

This article is a follow-up of Miyakoda and Sirutis (1977), which described the design of a performance test of the subgrid-scale (SGS) parameterization scheme in a general circulation model (GCM). Three versions of parameterization were selected, i.e., the A2, the E4, and the F2 physics. They were reasonably diverse in the formulation of concept and the extent of elaboration. They were also considered to represent a variety of the methods that had existed before 1975.

Since then, the similar kind of sensitivity tests or performance tests of the SGS parameterization have been conducted by several groups. Baker et al.

(1977; 1978) and Donner et al. (1982) compared two different convective parameterizations, i.e., the moist convective adjustment (Manabe et al., 1965) (referred subsequently to the Manabe scheme), and the modified Kuo scheme (Kuo, 1965; 1974), applying them to the NCAR (National Center of Atmospheric Research) GCM and the Community Climate Model, respectively. They found that the Kuo scheme warms the upper troposphere more than the Manabe scheme. Baker et al. obtained a substantial difference in kinetic energy, whereas Donner et al. obtained a smaller but measureable difference. These works are essentially sensitivity study, comparing two GCM runs of different moist convection schemes. On the other hand, Hollingsworth et al., (1980) carried out an extensive comparative forecast experiment of ECMWF (European Centre for Medium-Range Weather Forecasts) physics and GFDL 1965 physics (Manabe et al., 1965) where the former incorporates the modified Kuo method, surface flux scheme dependent on stratification, and the elimination of dry convective adjustment (Tiedtke et al., 1979). The conclusion was that little difference exists between two version physics in the quality for a 10 day forecast, although some differences are noted in the individual features such as the mean meridional circulation and meridional fluxes of momentum and sensible heat due to medium waves. Tiedtke's (1982; 1984) works are similar to the present paper except that his study is a sensitivity test. The unique aspects of his work are that not only the Kuo scheme but also the Arakawa-Schubert scheme are used, and that the interaction of model's cloud with radiation is included. He found that the cumulus cloud-radiation interaction plays a significant role in producing the zonal asymmetry of tropical heat sources and sinks.

In the present work, the 30 day forecast experiments with the three combinations of the SGS processes were performed. The preliminary study (Miyakoda and Sirutis, 1977) treated only individual effects such as the depth of mixed layer and the vertical distribution of heating and moistening. On the other hand, we will focus here on the collective effects of the parameterized processes. The assessment of various schemes with the observed data is the key aspect of this paper.

2. THE SPATIAL RESOLUTION AND THE SGS PROCESSES OF THE GCM

The GCM was the finite difference model using the modified Kurihara grid in which the Arakawa A-grid was employed and the kinetic energy conserving finite difference was included (Kurihara and Holloway, 1967; Umscheid and Bannon, 1977).

2.1 Various SGS processes

Concerning the SGS physics, one difference from Miyakoda and Sirutis (1977) is that the F3-physics instead of the F2-physics will be employed, where the treatment based on the mixed layer theory in the F2 was replaced by the turbulence closure scheme. Thus there are three versions of combined physics, i.e., the A2, the E4 and the F3 physics. However, for simplicity, we shall hereafter denote them by the A, the E and the F-physics. One more modification is the condensation criterion. The criterion for the A and the E model is now 80% relative humidity for practical reasons, and that for the F model remains at 100%.

It may be worthwhile to review briefly the models of these physics. The first model includes the A physics, which is the so-called "GFDL 1965 physics" (Manabe et al., 1965). This utilizes the drag law formulation of neutral stratification for surface fluxes, the mixing length theory, the dry convective adjustment, and the Manabe cumulus scheme.

The second model includes the E physics, which incorporates the similarity theory for the surface constant-flux layer and the turbulence closure scheme for the entire atmosphere, excluding the dry convective adjustment. The Manabe scheme is retained as the cumulus parameterization. This model contains three subsurface levels for soil heat conduction. The turbulence closure scheme is of the second-order at the hierarchy level 2.5 (Yamada and Mellor, 1980), which predicts the SGS turbulent intensity at all grid points but uses the diagnostic equation for the second moment of temperature fluctuation, and importantly, includes the "diffusion term".

The third model includes the F-physics which uses the E-physics as the base but replaces the Manabe scheme with the Arakawa-Schubert (1974) method, which uses the "penetrative convection" approach. In the previous F2-physics, the planetary boundary layer was treated by an integrated scheme based on Randall's (1976) mixed layer theory, whereas in the F3-physics, the planetary boundary layer was handled by the turbulence closure scheme, and the mixed layer depth is calculated as the "lifting condensation level" (see Appendix I).

The equations in the new F-model are written symbolically as

$$\frac{dT}{dt} = \omega \frac{RT}{p} + Q_R/C_p + g \frac{\partial H}{\partial p} + L \cdot C/C_p$$

$$+ (\text{cumul. conv.}) + \nabla (\kappa \nabla T), \qquad (2.1)$$

$$\frac{dq}{dt} = g \frac{\partial E}{\partial p} - C + (\text{cumul. conv.}) + \nabla(\kappa \nabla q), \qquad (2.2)$$

$$\frac{d\underset{\sim}{V}}{dt} = -\underset{\sim}{K} \times f\underset{\sim}{V} - \nabla\phi - g \frac{\partial \tau}{\partial p}$$

$$+ (\text{cumul. conv.}) + (\text{horiz. diff.}), \qquad (2.3)$$

where T, q and $\underline{V}$ are the temperature, the mixing ratio of water vapor, and the wind vector, respectively, H, E and τ are the vertical turbulent fluxes for heat ($\rho\ \overline{w'\theta'}$), moisture ($\rho.\overline{w'q'}$) and momentum ($-\rho\ \overline{w'u'}$, $-\rho\ \overline{w'v'}$), respectively, Q_R is the radiational heating, C is the rate of condensation due to large-scale processes, L is the latent heat, K is the coefficient of lateral turbulent diffusion, ∇ is the two-dimensional del operator, (cumul. conv.) denotes the effect of the Arakawa-Schubert cumulus parameterization, and other notations are conventional.

2.2 Further remarks on physics

The cloud-radiation interaction has not been treated at all in this study. Concerning the Arakawa-Schubert cumulus parameterization, the most recent version of code, provided by Lord, then at UCLA (Lord et al., 1982), was used throughout this research. Different from the previous version, the effect of "water loading" on the cloud buoyancy was removed. The detrainment from clouds is assumed to take place not only the cloud top but also beneath the top. The calculation of Fredholm's integral equation for "cloud mass flux" is efficiently carried out by solving a matrix with the "simplex method".

In connection with the turbulence closure theory, Mellor and Yamada (1977) proposed an equation to calculate a "master length scale" of turbulence, but our work still used the old length scale specification of Blackadar.

The land surface temperature was calculated by the heat balance equation in the previous papers. However, for economical reasons, the surface temperature is now calculated from a prognostic equation as

$$\frac{\partial \Delta \cdot C_S T_S}{\partial t} = R_n - H_s - L\ E_s + H_{soil} \qquad (2.4)$$

where T_S is the temperature at the ground surface, R_n is the net radiation, C_S is the heat capacity of the soil, Δ is the thickness of the soil (5 cm in practice) H_S and E_S are the upward fluxes of sensible heat and water vapor, and H_{soil} is the upward heat flux in the soil at the surface. In addition, the Monin-Obukhov similarity function in stable condition has been replaced by Hick's (1976) formula, where the original formula was specified by Clarke (1970) empirically. (See Carson and Richards, 1978)

2.3 The spatial resolution

In Miyakoda and Sirutis (1977) the N24L18 model was used, where N24 denotes the horizontal resolution and 24 indicates the number of gridpoint between the

pole and equator (the grid size is 3.75° in the meridional direction) and L18 denotes the 18 vertical levels. It is our view that the spatial resolution and the SGS physics are, in addition to the radiation, the major factors which determine the overall quality of the GCM. Figure 1 shows the performance of various models which consist of different resolutions and different physics. There are the N24L18, the N48L9 and the N48L18 models, and there are the A, the E and the F physics.

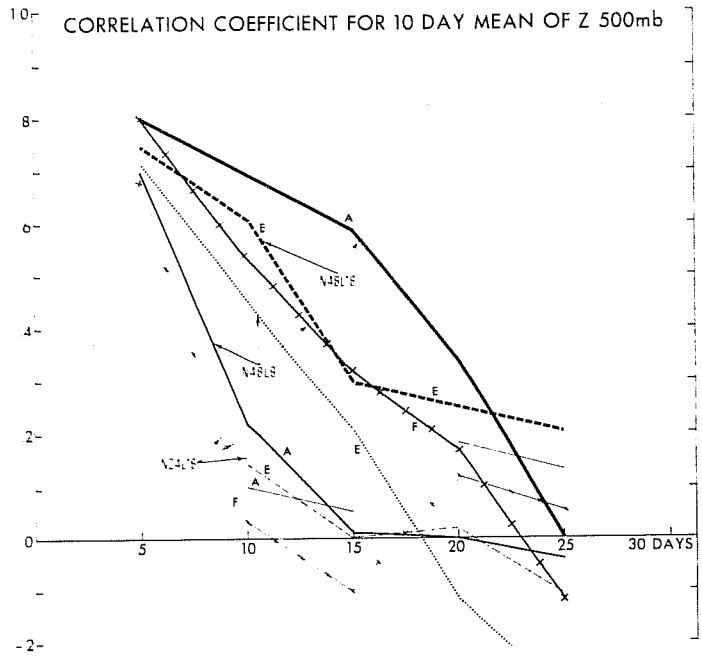

Fig. 1. Correlation coefficients between the forecast and the observed anomalies of 10 day mean geopotential height for the northern hemisphere (90°-25°N) in the case of March 1965. Thinner lines, thin lines and thick lines are for the different spatial resolution models, i.e., N24L18, N48L9, and N48L18, respectively for three different SGS parameterizations. The N48L18 does not include the F-physics.

The predictive performance is shown by the correlation coefficients of the anomaly of the 10 day mean geopotential height at 500 mb level. The experiment was applied for the case of March, 1965. The correlation curves are plotted for one-month from 1 to 31 March. The figure may indicate that the curves of various resolution models are clustered together irrespective of the physics, indicating that the resolution is more dominant and important factor than the SGS physics. For example, the N24L18 models are all marginal; the difference of the SGS physics can not be well recognized beyond Day 10 and the N24L18 models show virtually zero skill for all physics. The performance of the models is, in the ascending order, the N24L18, the N48L9 and the N48L18, though they are not exactly in this order for other verification variables such as the azonal eddy kinetic energy. It has been known, however, that in order to obtain beneficial

impact of the SGS physics, the GCM should have sufficiently fine space resolution. Otherwise, the model is insensitive to the difference of physics.

In the forthcoming sections, we will use mostly the N48L9 models, since the higher resolution models are prohibitively expensive to run. As will be shown later, the N48L9 model (1.875° grid size in the meridional direction) gives reasonably good (but not entirely satisfactory) results for monthly forecasts so far as the troposphere is concerned.

3. THE OUTLINE OF EXPERIMENTS

One-month integrations for 5 cases were performed by the three versions of model, i.e., the A, the E and F-physics using the N48L9 resolution. In a separate project which treated the simulation of January 1977 blocking event (Miyakoda et al., 1983) it was found that the second model (E) was successful in producing the blocking ridge, while the first model (A) did not perform well. Thus, the objective of this paper is to confirm the hierarchy of the performance assessing the GCM solution for the purpose of medium-range deterministic prediction and of monthly time-mean forecasts, based on 5 cases in this paper, but 8 cases in the near future. The impact of cumulus parameterization, which was not included in Miyakoda et al. (1983), is also investigated.

Five cases for different initial conditions were employed, i.e., 00GMT, 1 March, 1965; 00GMT 1 January, 1977; 00GMT 1 January, 1979; 00GMT 16 January, 1979; and 00GMT 24 August, 1974. All data are the global sets, in which the data of $\underset{\sim}{V}$, T, q (mixing ratio of water vapor) and P_s (sea level pressure) are included. The first case is the manual analysis, that is, the same as used in Miyakoda and Sirutis (1977). The second, the third, and the fifth cases were obtained by the GFDL four-dimensional data assimilation system (Ploshay et al., 1983; Miyakoda et al., 1982). The fourth case was produced by ECMWF (see Bengtsson, 1981).

In order to make an appropriate assessment on the SGS parameterization, the quality of initial condition is important together with the sufficient spatial resolution of the GCM. The quality of initial data has been substantially improved recently.

The verification for the 30 days was made using the NMC (National Meteorological Center) analysis for January 1977 and 1979. The verification data for March 1965 was supplied by NMC, and by Oort (1983b).

4. THE SUMMARY OF 4 CASES

4.1 Skill scores

Figures 2, 3 and 4 are summaries of verification for the 10 day means of geopotential height at 500 mb and 1000 mb levels. The curves indicate arithmetic averages of the skill scores for four winter and one spring cases.

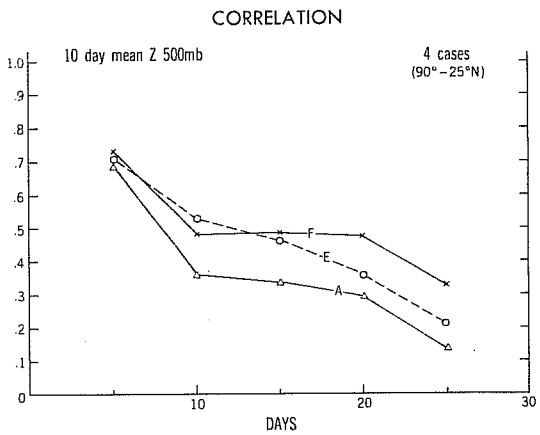

Fig. 2. Correlation coefficients between the forecast and the observed anomalies of 500 mb 10 day mean geopotential height for the northern hemisphere (90°-25°N). The curves are the averages of the four cases.

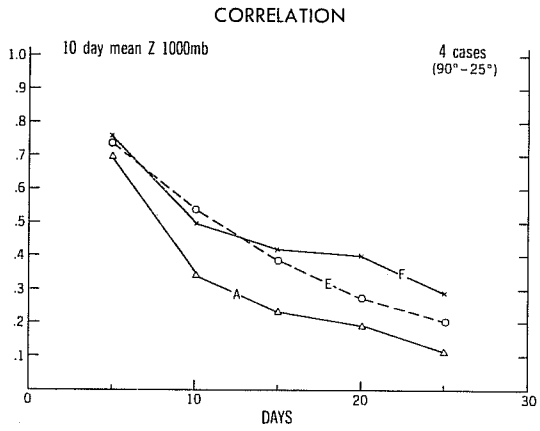

Fig. 3. The same as figure 2 but for 1000 mb.

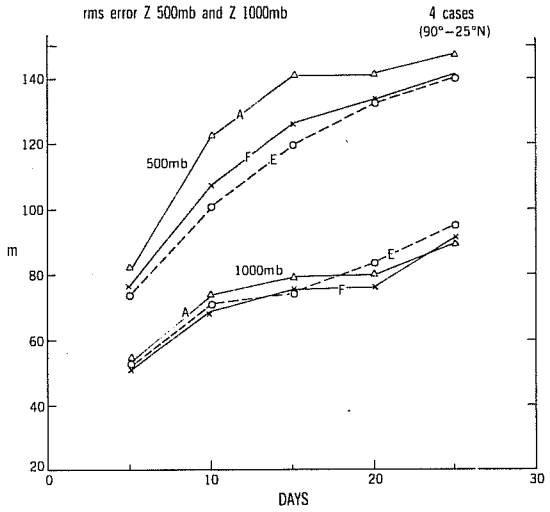

Fig. 4. Root-mean-square errors of the 500 and 1000 mb 10 day mean geopotential height for the northern hemisphere (90°-25°N). The curves are the averages of the four cases.

The scores are: correlation coefficients of the height anomalies (the departure from climatology) between forecasts and observation, and the root-mean-square errors of height, the verification domain being the northern hemisphere poleward of 25°N. Figures 2 and 3 are the correlation coefficients for the 500 mb and 1000 mb height, respectively. Figure 4 is the root-mean-square error for both 500 mb and 1000 mb height.

In the first ten days, the scores are high for all cases and for all models. Beyond Day 10, they start to decay depending upon the cases and also upon the models. In the first ten days, the hierarchy of the performance is, in descending order: the F, the E and the A for all scores except the rms error of 500 mb height. This is the extent to which the SGS processes (which we employed) can contribute to the improvement for medium-range forecasts. For the correlation coefficient of 500 mb geopotential height, for example, the F-model yielded better results than the A-model by 0.05.

Beyond Day 10 and up to Day 20, the overall hierarchy of the performance is, in the descending order: the F, the E and the A or the E, the F and the A for the scores of height at 500 mb.

4.2 Prognostic geopotential height maps

As sample of the forecasts, the 500 mb geopotential height maps at Day 10 and Day 20-30 are shown and compared with the observation. The Day 10 maps are the snapshots, whereas the latter are the 10 day means. Day 30 is beyond the limit of the deterministic predictability, and therefore, the temporal mean maps are appropriate for comparison with reality.

The 500 mb geopotential height maps

Figures 5 and 6 are for March, 1965, in which the Alaskan blocking ridge is included. On March 20, the sudden warming and the vortex breakdown occurred in the stratosphere. The Pacific block at 130°W stayed throughout the entire month in the observation. The F-model simulated well the maintenance of the ridge. In figure 5, at Day 10, all models gave reasonable forecasts. In figure 6, at Day 20-30, the F is good.

Figures 7 and 8 are for January, 1977, in which the extraordinary cold and warm air prevailed over North America. Pronounced blocking ridges over both Pacific and Atlantic were persistent for several months. The Pacific block at 140°W persisted up to Day 25, and it then started to move westward. There are appreciable number of transient waves that propagate eastward. In figure 7, at Day 10, the E and the F are very good. In figure 8, at Day 20-30, the F and the E are good, while the A is poor. The maintenance of the blocking ridge was better simulated by the E and the F than the A.

Figures 9 and 10 are for the case of 1 January 1979. This and the next cases are for the Special Observing Period of FGGE. In the first half of January, Pacific blocking was dominant, and in the latter half, European blocking emerged and persisted. In figure 9, at Day 10, the F and the E are good, whereas the A is poor for the sector 180°-120°W. In figure 10, at Day 20-30, the E is good, and the F is not bad, whereas the A remains poor.

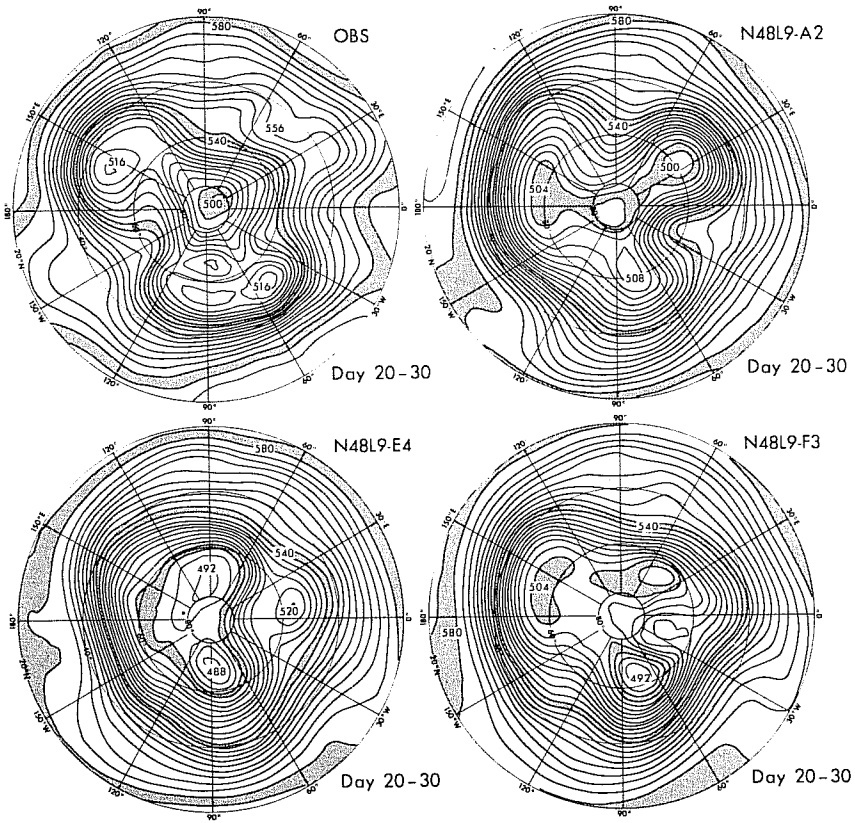

Fig. 6. 500 mb 10 day mean geopotential height maps with 40 meter intervals of the contours for Day 20-30 in the case of 1 March 1965. The observation (upper left), the A (upper right), the E (lower left), and the F (lower right).

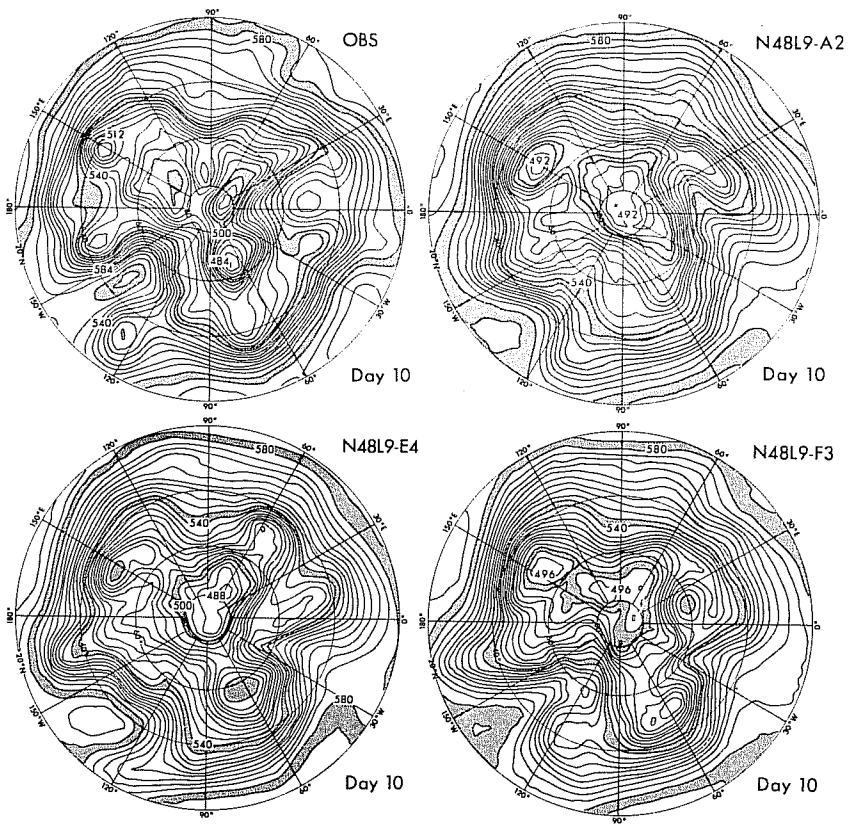

Fig. 5. 500 mb geopotential height maps with 40 meter intervals of the contours at Day 10 for 1 March 1965. The observation (upper left), the A (upper right), the E (lower left), and the F (lower right).

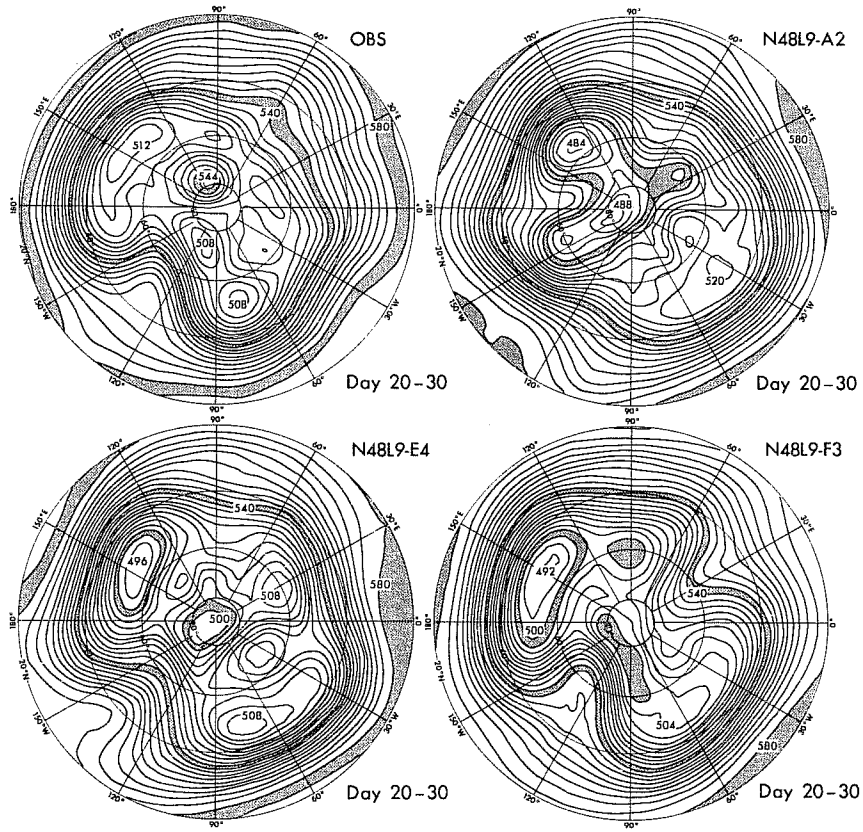

Fig. 8. The same as figure 6, but for 1 January 1977.

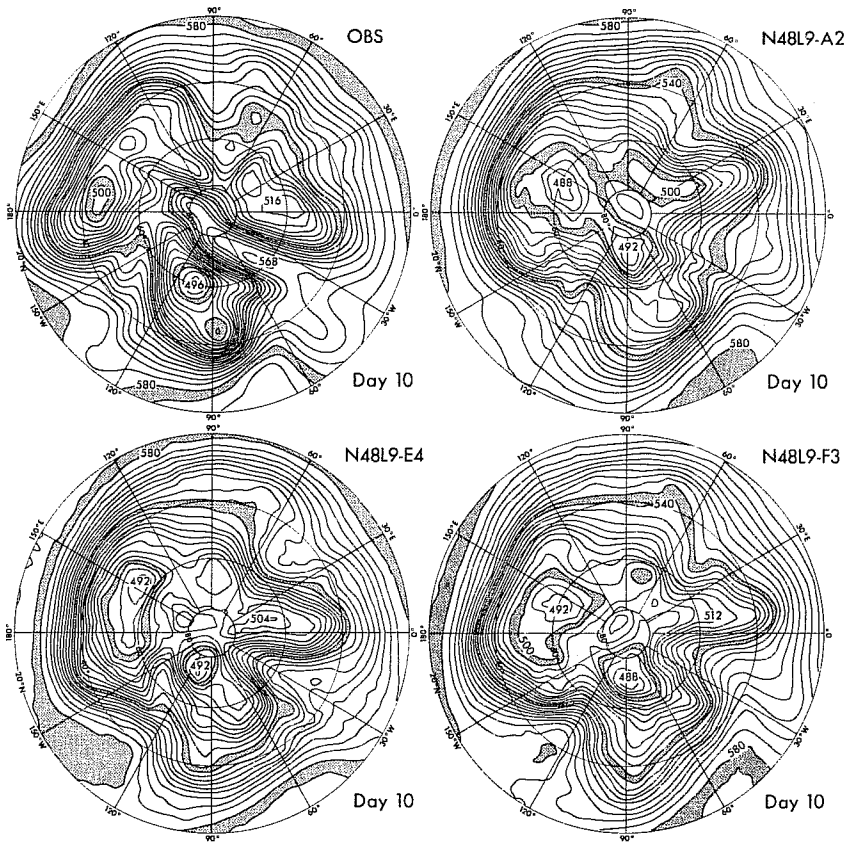

Fig. 7. The same as figure 5, but for 1 January 1977.

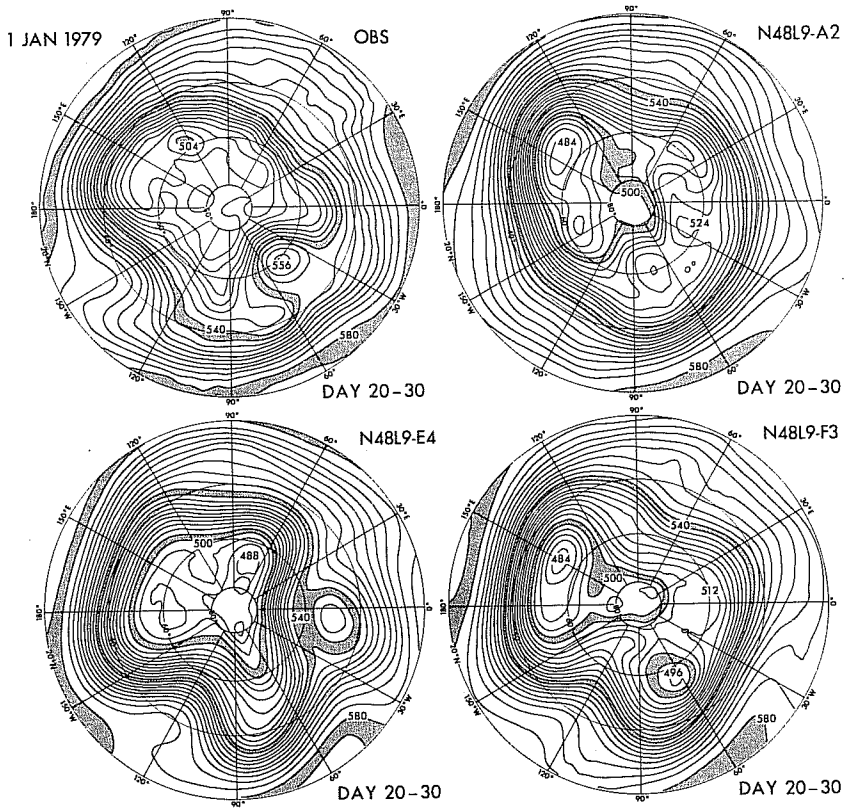

Fig. 10. The same as figure 6, but for 1 January 1979.

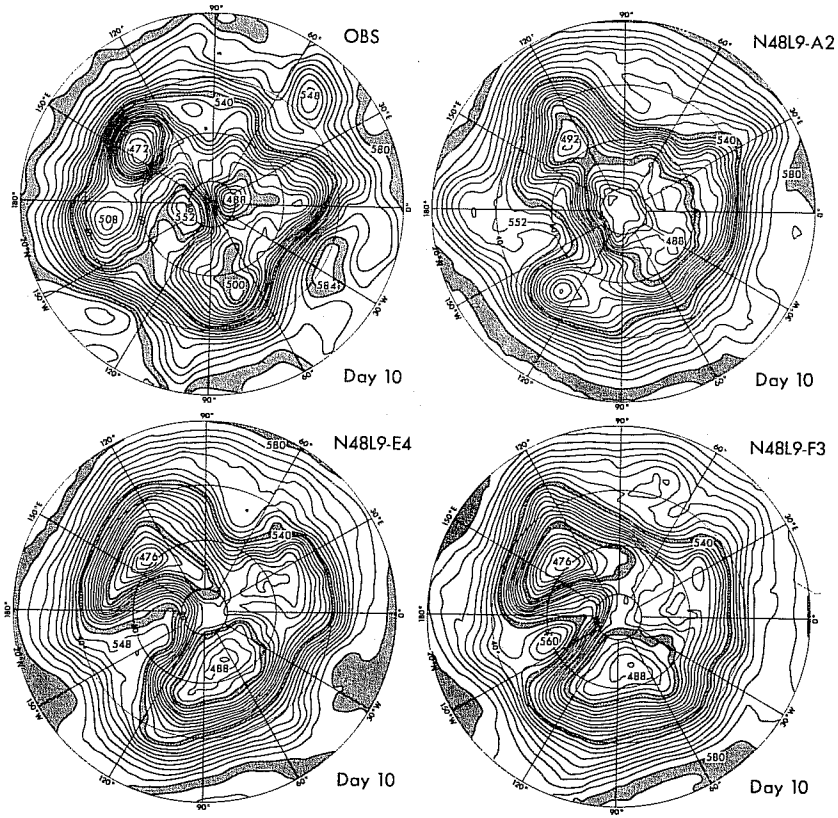

Fig. 9. The same as figure 5, but for 1 January 1979.

Figures 11 and 12 are for the case of 16 January, 1979, in which only the Atlantic blocking ridge persisted between 30° - 60°W longitude. This case was treated by ECMWF, and an excellent forecast was obtained by the ECMWF model, using the same data as in this study (Bengtsson, 1981). In figure 11, at Day 10, the E, the F and the A are all very good. In figure 12, at Day 20-30, the F is very good; the A is not bad, but the E is poor.

In summary, blocking ridges at 40° - 60°N were well simulated by the E or the F. The amplitude of meandering westerlies tend to be larger in the E or the F than in the A. The performance of the A was poor for this type of situation; blocking ridges became weak and disappeared. Day 10 is the target day in the medium-range forecasts, which corresponds to the latter part in the deterministic predictability range. These experiments indicate the SGS processes contribute, in this extent, to these forecasts. It may be noticed, however, that the prognostic maps of the A, the E and the F-models for Day 20-30 are more similar to each other than those to the observation.

4.3 Simulated general circulation

The 30 day means of various variables in the models' results were calculated and compared with the corresponding observations. The presentation will be divided into five variables, i.e., zonal averages of the temperature, the zonal wind, the meridional wind, the vertical pressure velocity, and the squared vertical pressure velocity.

(a) Temperature

The ensemble averages over three cases of temperature difference of the A, the E and the F predictions from the observation are shown by meridional sections in figure 13, the three cases being 1 January, 1977, 1 January, 1979, and 16 January 1979. The following are noted.

- Error distributions are similar among the three models, indicating that there is a large source of common errors, which appears not well treated in these models.

  The predicted temperature is overall lower than the observation. Particularly the temperature deficits are extremely large at high latitudes. It has long been speculated that poleward eddy heat fluxes are not sufficiently strong to compensate for these deficiencies
- It is surprising that the difference between the E and the A is so small, so far as the zonal average and monthly mean temperature is concerned.
- The F-model has a pronounced tendency of warming in the upper layer centered at 200~250 mb, and of cooling beneath it at 400 mb. The warmings are spread for the meridional region of 40°N - 40°S.

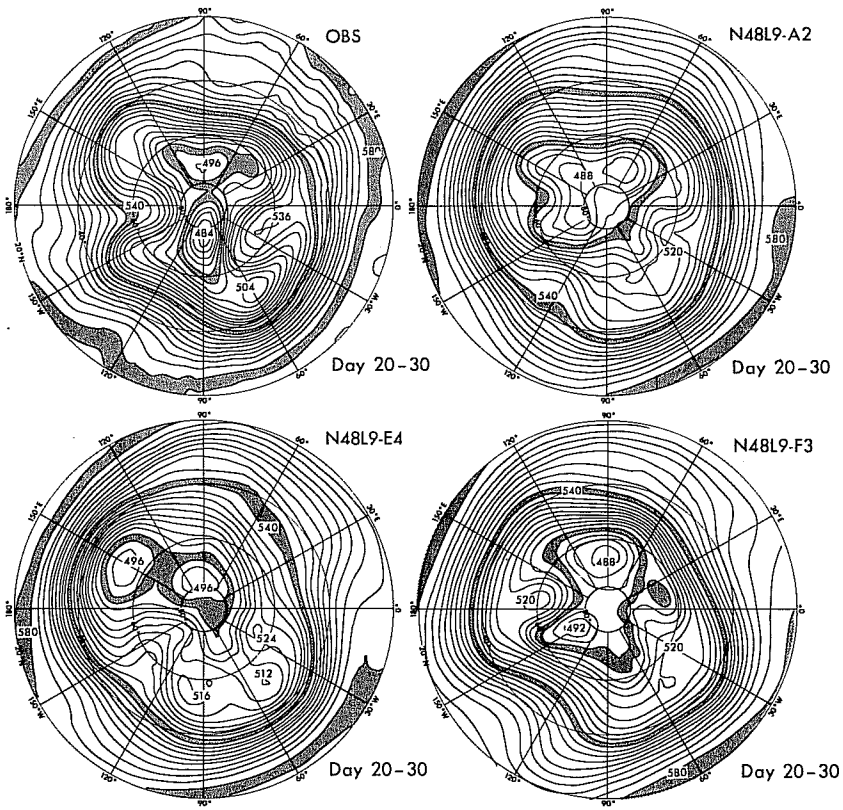

Fig. 12. The same as figure 6, but for 16 January 1979.

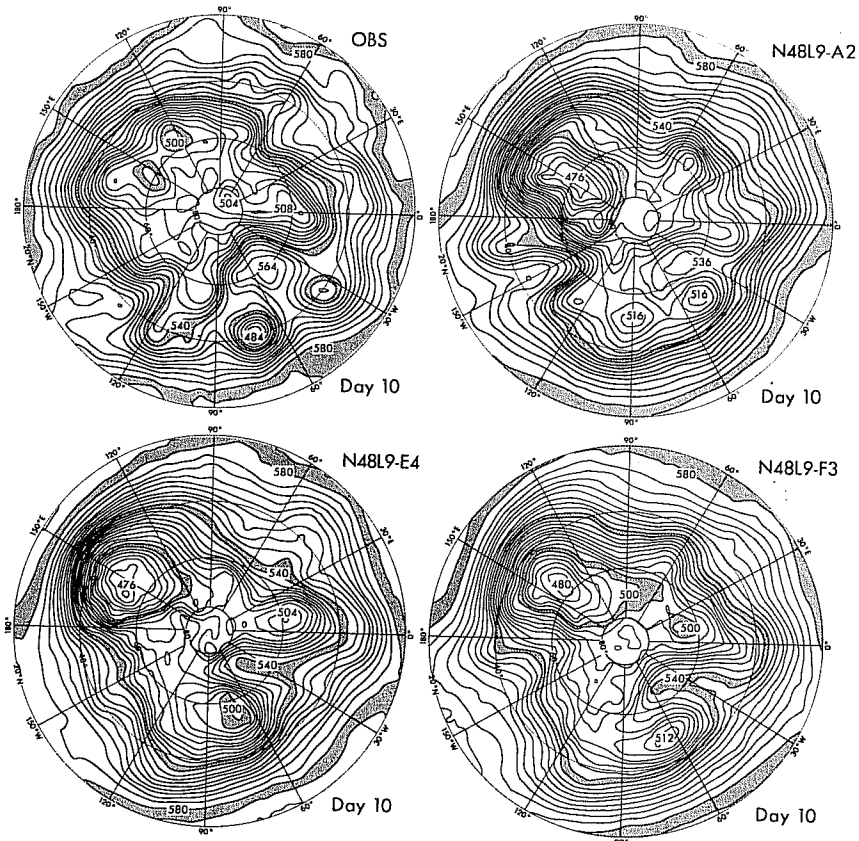

Fig. 11. The same as figure 5, but for 16 January 1979.

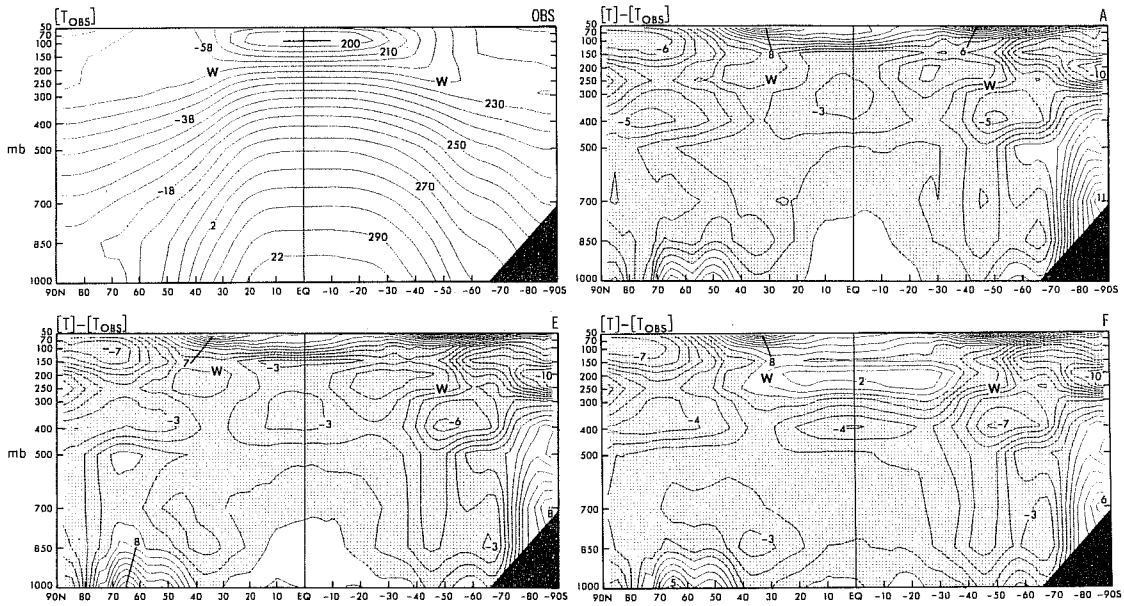

Fig. 13. The monthly-mean, zonally-averaged temperature difference between the prediction and the observation, i.e., the A (upper right), the E (lower left), and the F (lower right), with the contour interval of 1°C. The total temperature is also shown at the upper left with the contour interval of 5°K. All diagrams are the ensemble mean of three January cases. The abscissa is the latitude, and the ordinate is the pressure in mb, both at equal interval. The negative regions are shaded. The positions of subtropic westerly jets are indicated by W.

It was discussed in Miyakoda and Sirutis (1977) that the F gives more heating at high levels than the A and the E, because of the penetrative convection characteristic in the Arakawa-Schubert scheme. Figure 13 reproduces exactly this tendency. The fact was also pointed out by Baker et al. (1977), Hollingsworth et al. (1980), Donner et al. (1982), Rowntree (personal communication) and Tiedtke (1983), comparing the GCM results between the Manabe scheme and penetrative convection schemes, where the first three papers used Kuo or modified Kuo schemes, Rowntree used the UK Met. Office cumulus parameterization (Lyne and Rowntree, 1976) and Tiedtke used both the Arakawa-Shcubert and the Kuo schemes as the penetrative convection parameterization.

The point, being that the upper layer heating,is the most fundamental feature in the penetrative convection, which leads to various consequences for the general circulation.

(b) Zonal wind

The ensemble averages of zonal wind difference of the A, the E, and the F predictions from the observation for the three January cases are shown by meridional sections in figure 14. The following are noted.

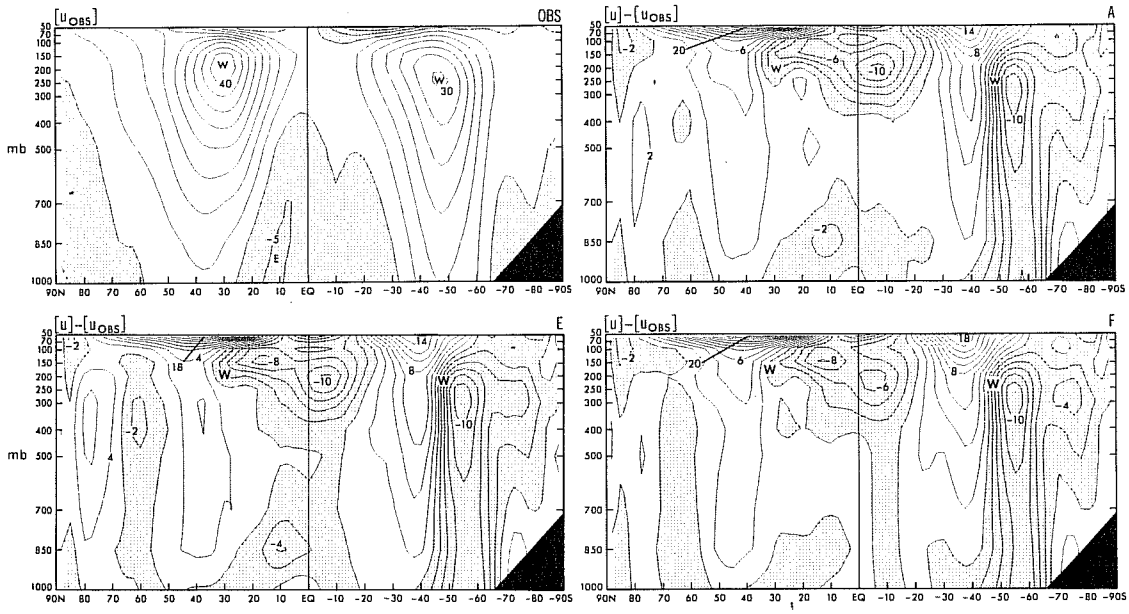

Fig. 14. The monthly-mean, zonally-averaged zonal wind difference between the prediction and the observation, i.e., the A (upper right), the E (lower left), and the F (lower right), with the contour interval of 2 m.s^{-1}. The total zonal wind is also shown at the upper left with the contour interval of 5 m.s^{-1}. See the caption 13 for other explanation.

- In this case also, error distributions are similar among the three models. The major cause would be the same as for the temperature.
- In all models, the westerly jets are overly intensified, and are shifted sli ghtly to poleward in the northern hemisphere, and considerably to equatorward in the southern hemishpere.
- In all models, easterly winds at the upper levels (200mb) in the equatorial region are excessively strong. In the F-model, this easterly bias is appreciably moderated.

Hollingsworth et al. (1980) and Donner et al. (1982) mentioned that the intensity of westerlies in winter is unfavorably increased at the midlatitudes by the Kuo scheme compared with the Manabe scheme. This feature may or may not agree with our result. Tiedtke's (1982) result is similar to our results in Figure 14.

(c) Meridional wind

The ensemble averages of meridional wind of the A, the E, and the F predictions for the three January cases are displayed together with the climatology by meridional section in Figure 15. The climatological values were taken from Oort (1983) based on 10 year data. The following are noted.

- Distributions of zonally-averaged meridional winds, [v], are similar to each other among the models. The Hadley cell circulations are outstanding, and the three circulation cells are recognized in both hemispheres.

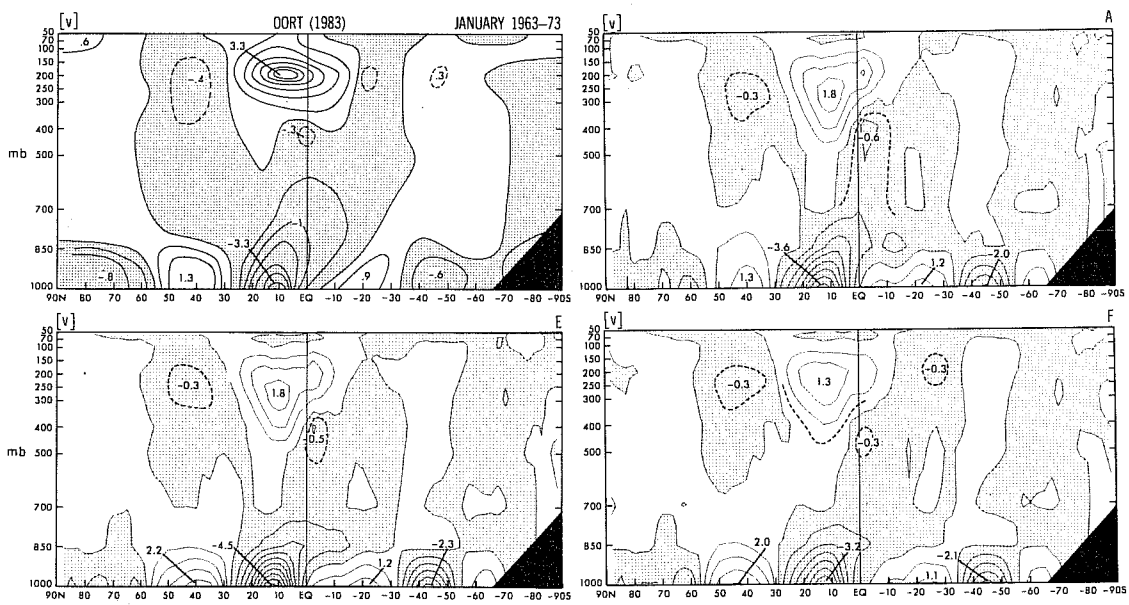

Fig. 15. The monthly-mean, zonally-averaged meridional wind of predictions, i.e., the A (upper right), the E (lower left), and the F (lower right), and the climatology for January (upper left) with the contour interval of 0.5 m.s^{-1} in solid lines and of 0.25 m.s^{-1} in dashed lines. See the caption 13 for other explanation.

o The center of the upper level tropical current is located at 10°N and 250 mb level in the predictions with the intensities 1.8 m.s^{-1} (the A), 1.8 m.s^{-1} (the E) and 1.3 m.s^{-1} (the F), whereas the climatological center is at 10°Nand 200 mb level with the intensity 3.3 m.s^{-1}; it is larger by a factor 1.5~2. It is noted that the F model decelerates the meridional wind, [v], and that the weaker equatorial cross current, in turn, affect the intensity of zonal wind, [u], as is seen in Figure 14.

The effect of the "cumulus friction" was discussed by Holton and Colton (1971), Stone et al. (1974) and Schneider and Lindzen (1976). One of the possible consequences of this effect is the intensification of the winter Hadley circulation (Schneider and Lindzen, 1976; Helfand, 1979). Helfand (1979) reported 14% increase in the [v] of his GCM with the cumulus friction, compared with the case without it. In this connection Figure 15 shows the opposite. The deceleration of [v] in the F is due to the decrease of condensation in the tropics. Donner et al. (1982) mentioned that the poleward flux near 200 mb in the tropics decreases by ~0.9 m.s^{-1} in the Kuo scheme compared with the Manabe scheme. So this result agrees with the present paper, though Donner et al. does not include the cumulus friction.

o The tropical surface counter current of the Hadley cell is located at 12°N with the intensity - 3.6 m.s^{-1} (the A), -4.5 m.s^{-1} (the E) and -3.2 m.s^{-1} (the F), whereas the climatological current is at 10°N with

the intensity -3.3 $m.s^{-1}$. This result indicates that the E-physics intensifies the surface counter current substantially, and the F-physics decelerates it.

- The surface currents outside of tropics are weaker, and yet measurable. The climatological values are very weak. Oort and Peixoto (1983) stated that the [v] values for the Ferrel cell are very hard to measure directly. It is interesting to note that the E-physics accelerates appreciably these surface currents in the extratropics too.

(d) Vertical velocity at 660 mb

The zonally averaged vertical pressure-velocity,

$$\omega \left(\equiv \frac{dp}{dt} \right)$$

at 660 mb level is shown in figure 16. There is the upward velocity at the equatorial zone and downward velocity at the doldrum zone.

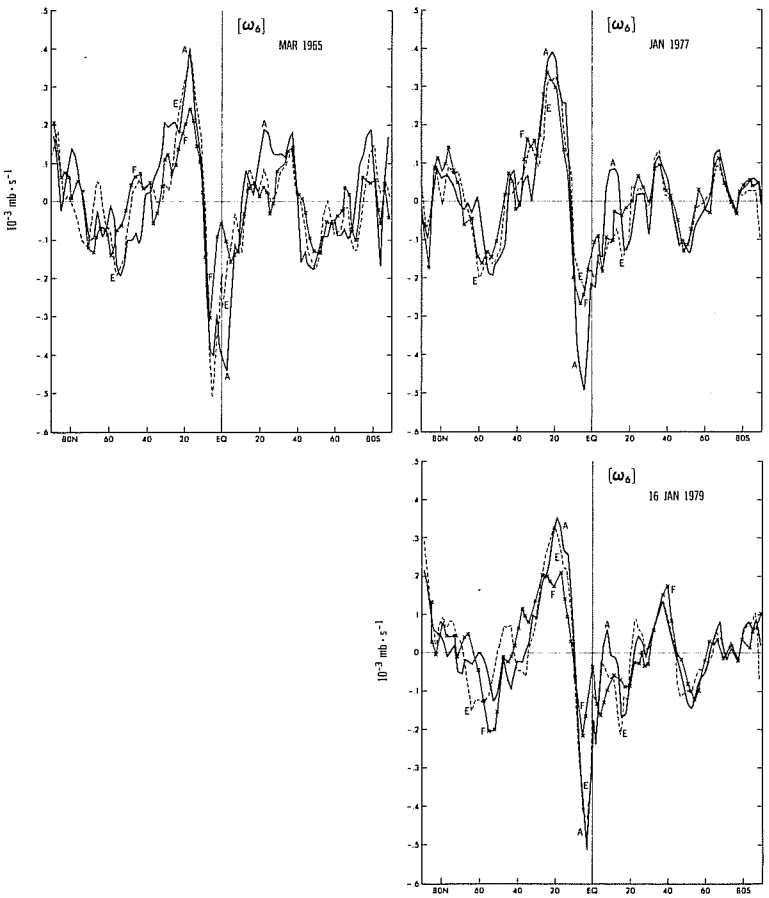

Fig. 16. Monthly and zonal average of vertical pressure velocity ω at model's level 6 (660 mb). The case, c, of 1 January 1979 is missing.

Comparison of these values with the climatological values by Oort (1983) has revealed that $[\omega]$'s at 5°N are: -.5 (the A), -.3 (the E), -.2 (the F) and -.19 (climate); and $[\omega]$'s at 20°N are: .37 (the A), .32 (the E), .27 (the F) and .2 (climate) in units of 10-3 mb.s-1. The agreement is overall good, despite the difficulty of direct measurement.

In summary, the intensities of predictions are strongest in the A-model, and weakest in the F-model. It is considered that two factors mainly contributed to this feature, i.e., the "penetrative convection" by the Arakawa-Schubert scheme, and the difference of the surface heat exchange and soil heat conduction. This tendency agrees with that of Baker et al. (1977) and Donner et al. (1982).

(e) Squared vertical velocity

Figure 17 presents the squared vertical velocities, ω^2, averaged vertically, and zonally, which are perhaps the most pronounced feature, next to the static stability, of the impact of the Arakawa-Schubert perameterization. The ω^2 is consistently lowest in the F compared with the E and the A. This tendency is particularly strong in the tropics, implying that the F-model produces the spatially and temporarily smooth vertical velocity, and accordingly, smooth distribution of rainfall.

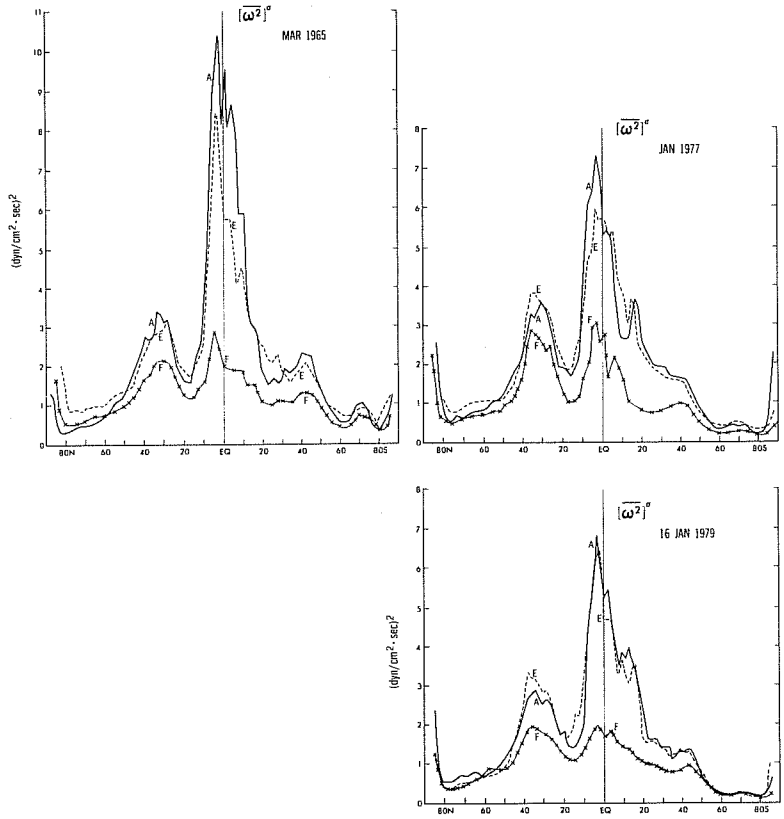

Fig. 17. Monthly, vertical, and zonal average of squared vertical pressure velocity, ω^2. The case, c, of 1 January 1979 is missing.

The low value of ω^2 in the F, would be resulted from the filtered cloud mass flux and the stabler thermal stratification, suppressing high-frequency gravity waves.

(f) Sector mean zonal wind

It is now understood that the meridional profile of the zonal wind is extremely important for determining planetary-scale wave patterns (Held, 1982; Miyakoda et al., 1983; Kinter and Miyakoda, 1983). Even small modulation of zonal wind profile causes a substantial change in downstream meandering of westerlies in conjunction with the orography (see Appendix II).

According to the study of Kinter (1983), the zonal winds, that are possibly related to the Pacific teleconnection pattern, i.e., PNA (Wallace and Gutzler, 1981), are the longitudinally averaged winds over the sector of 90°E - 180° - 90°W, and the zonal winds related to the Atlantic teleconnection pattern, i.e., WA, are the ones over the sector of 170°W - 0° - 10°E.

Figures 18 show the differences of sector means of zonal wind between the predictions and the observations (i.e., the errors of zonal wind). Figures 18a and b are the averages over the Pacific sector for two cases, and figures 18c and d are the averages over the Atlantic sector for other two cases.

These diagrams together with the flow patterns in figures 6, 8, 10 and 12 appear to reveal a certain tendency, suggesting a link between the zonal wind and the teleconnection index, and possibly the blocking activities. Namely, the observed 10 day mean flow patterns in the upper left of figure 6 (March 1965) and 8 (January 1977) are categorized as the positive PNA, and the patterns in the upper left of figure 10 (1 January 1979) and 12 (16 January 1979) are categorized as the positive WA.

In figure 18a, the intensities of [u] for the latitudinal region of 40°-70°N in the F is weaker than those of the A and the E, corresponding to the fact (figure 6) that the blocking ridge over Alaska (180° - 120°W) (positive index) is more easily reproduced in the F than in the E or the A. Similarly, the intensities of [u] in figure 18b in the E and the F are appreciably weaker than that of the A, corresponding to the blocking ridges in figure 8. The similar relation may be found in the cases of figure 18c and d and figures 10 and 12, respectively, for the Atlantic sector and WA patterns.

5. THE ENERGETICS

For the purpose of long-range forecasts, the monthly mean circulation pattern is of a considerable interest, because the time-mean fields are only predictable, if anything can be predicted, and the day-to-day variability is not

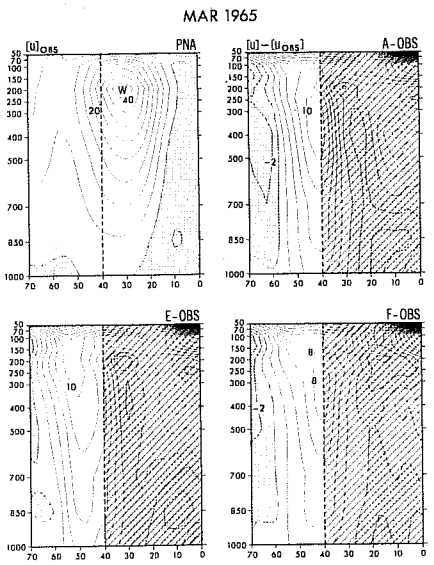

Fig. 18a. Sector mean of zonal wind over the longitudes of 90°E-180°-90°W, averaged over a month for the case of March, 1965. The observed zonal wind (upper left) with the contour interval of 5 m•s^{-1}. The difference between the prediction and the observation for the A (upper right), the E (lower left), and the F (lower right) with the contour interval of 2 m•s^{-1}. The negative regions are shaded.

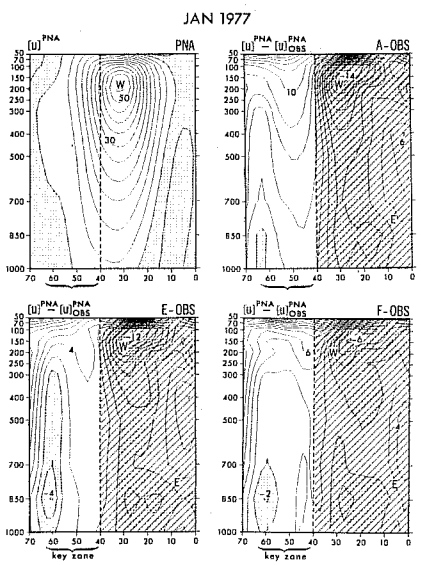

Fig. 18b. The same as figure 18a but for the case of January 1977. The averaging sector is: 90°E-180°-90°W.

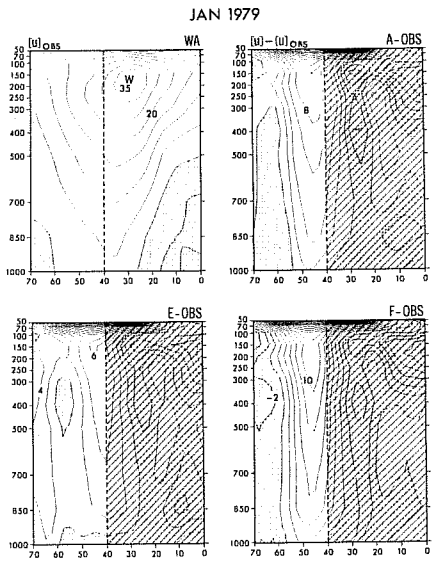

Fig. 18c. The same as figure 18a but for the case of 1 January 1979. The averaging sector is: 170°W-0°-10°E.

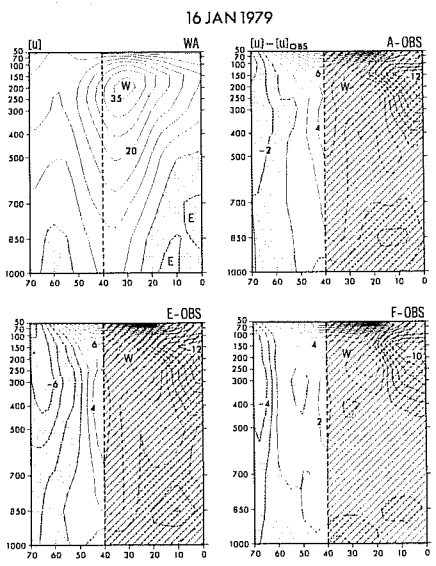

Fig. 18d. The same as figure 18a but for the case of 16 January 1979. The averaging sector is: 170°W-0°-10°

expected to be simulated in detail. The monthly mean component of energy is expressed by the "stationary eddy kinetic energy", and the deviated part is by the "transient eddy kinetic energy".

5.1 The total kinetic energy

Kinetic energies are now divided into the zonal mean, [ ], and the deviations, i.e., the eddy ( )*, using the Oort's (1983) notations. For the purpose of separation the momentum is first divided as

$$u = [u] + u^* \tag{5.1}$$

$$v = [v] + v^* \tag{5.2}$$

thus

$$\overline{K}^H = \overline{K_M}^H + \overline{K_E}^H \tag{5.3}$$

where $\overline{(\ )}^H$ is the horizontal average over the entire domain,

$$K_M = \overline{K_M}^H = \frac{1}{2}\left(\overline{[u]^2}^H + \overline{[v]^2}^H\right) \tag{5.4}$$

$$K_E = \overline{K_E}^H = \frac{1}{2}\left(\overline{u^{*2}}^H + \overline{v^{*2}}^H\right) \tag{5.5}$$

Figures 19 show the vertical distributions of K_M and K_E averaged over the northern hemisphere (90° - equator). There are a number of salient features worthy to note.

- In the observation, K_M is substantially larger than K_E at their peaks. However, if the energies are integrated in the vertical, $\hat{K}_E$ is larger than $\hat{K}_M$ where $\hat{(\ )}$ is the mass weighted vertical average; $\hat{K}_E/\hat{K}_M = 1.02$. This value is quite reasonable in view of $\hat{K}_E/\hat{K}_M = 1.16$ for the 15 year January average (Peixoto and Oort, 1974). These two features are, to some extent, simulated by all models, i.e., $\hat{K}_E/\hat{K}_M$ = 0.74 (the A), 0.82 (the E), and 0.70 (the F).
- The maximum of energy is located at higher level for K_M say 200 mb, than for K_E say 250 ~ 300 mb (see also Peixoto and Oort, 1974). All models are successful in reproducing this aspect.

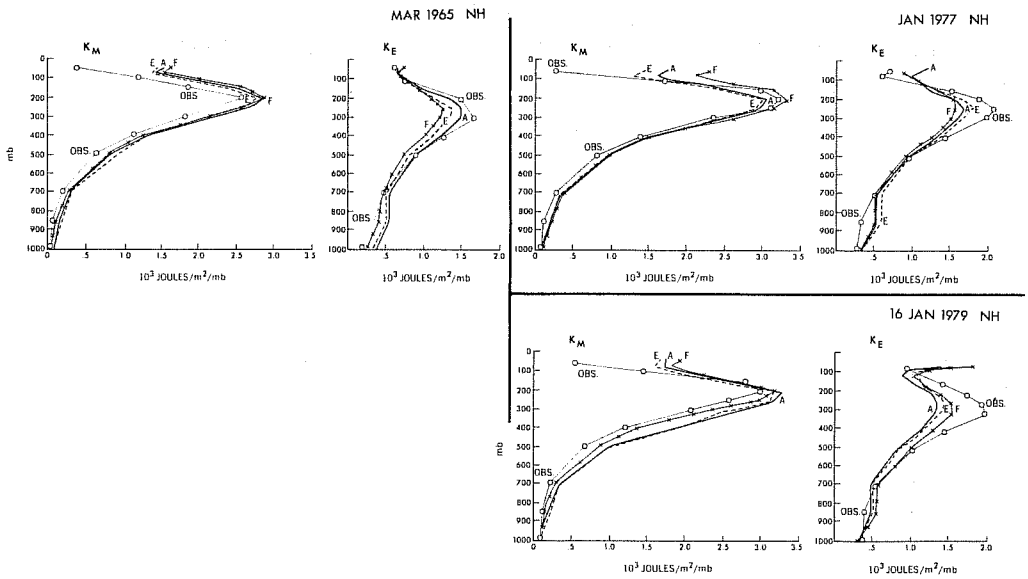

Fig. 19. Vertical distributions of the zonal mean kinetic energy, K_M (left) and the eddy kinetic energy, K_E (right), which are averaged horizontally over the northern hemisphere and over a month. The case, c, of 1 January 1979 is missing.

- For K_M the predictions appear often larger than the observation, whereas for K_E the predictions are always smaller than the observation. As will be seen later, the intensity of K_E for the southern hemisphere is, in the descending order, the observation, the A, the E, and the F-models.
- It is interesting to note that, in K_E there is a miximum at 850 mb level in the forecasts, whereas the counterpart is not found in the obsevation of NMC. Note, however, that there appears a maximum in the ECMWF analysis of FGGE, i.e., Figure 11 of Tiedtke (1983).

5.2 The eddy kinetic energy

The eddy kinetic energy, K_E, is further broken down into the stationary component and the deviation, i.e., the transient component. For example,

$$u^* \equiv \overline{u}^* + u' \tag{5.6}$$

where $\overline{(\ )}$ is the monthly mean and $(\ )'$ is the deviation from the mean. Thus

$$K_E = K_{SE} + K_{TE} \tag{5.7}$$

where K_{SE} is the stationary eddy kinetic energy and K_{TE} is the transient eddy kinetic energy, i.e.,

$$K_{SE} = \frac{1}{2}\left(\widehat{[u^*]}^2 + \widehat{[v^*]}^2 \right) \qquad (5.8)$$

$$K_{TE} = \frac{1}{2}\left(\widehat{[u'^2]} + \widehat{[v'^2]} \right) \qquad (5.9)$$

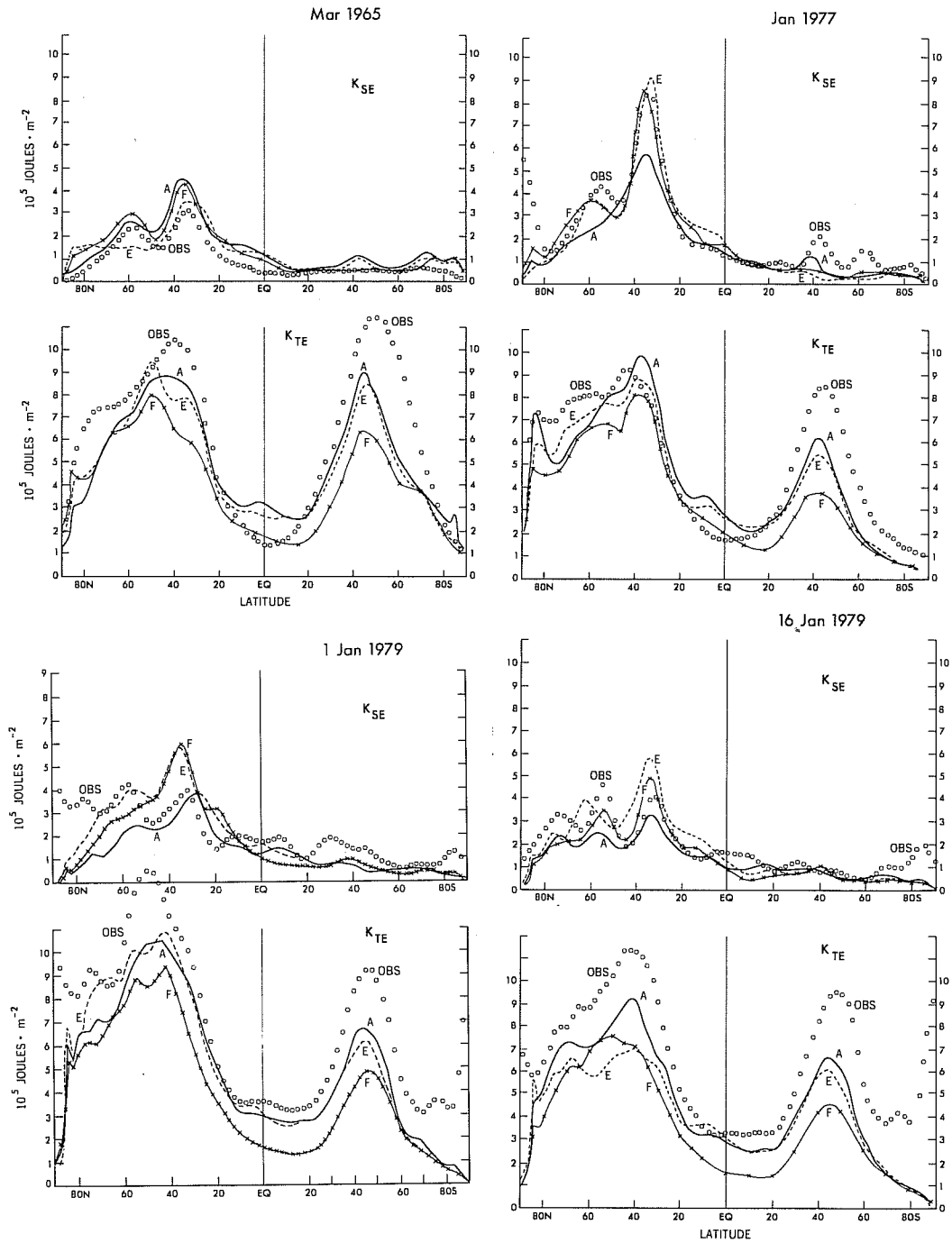

Fig. 20. Latitudinal distributions of the stationary eddy kinetic energy K_{SE} (upper) and the transient eddy kinetic energy, K_{TE} (lower), which are averaged vertically, zonally and over a month.

The 30 day mean of zonally averaged eddy kinetic energy for the three models' results and the observation is shown for all cases. Figures 20 a, b, and c are the stationary (K_{SE}) and transient (K_{TE}) eddy kinetic energies; all eddy energies are integrated in the vertical.

Figure 21 is the vertical distribution of K_{SE} and K_{TE}; all eddy energies are integrated over the Northern Hemisphere and are the average of two January cases, i.e., 1 January 1977 and 16 January 1979.

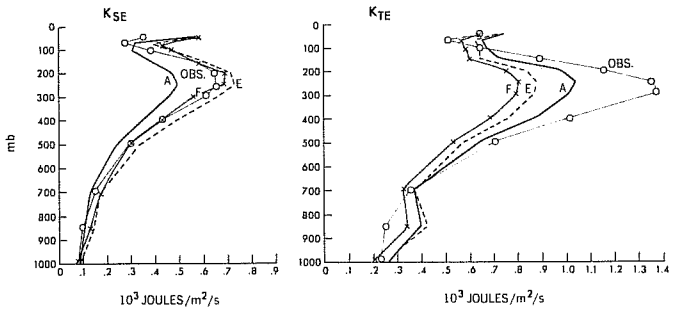

Fig. 21. The vertical distribution of the stationary eddy kinetic energy, K_{SE} (left), and the transient eddy kinetic energy, K_{TE} (right), for the mean of two year cases, i.e., January 1977 and 16 January 1979, which are averaged horizontally for the entire globe and over a month.

To summarize figures 20 and 21, we note the followings:

- For K_{SE} in the northern hemisphere, there are at least two maxima at latitudes of 35° and 55°, associated with the subtropical and the subpolar jets, respectively. See also Oort and Peixoto (1983; in their 15 year data, the peaks are at 30° and 55°N). The eddy kinetic energy at 55°N is related to blocking activities. According to the ECMWF FGGE analysis (Tiedtke, 1982), the maximum at 55°N consists of wavenumber 1-3 for large portion with the center at 60°N and of wavenumber 4-9 for another large portion, which is extended from 35°N.
- The latitudinal positions and magnitudes of K_{SE} are better predicted by all models in the northern hemisphere than in the southern hemisphere.
- The prediction of K_{SE} in the northern hemisphere is overall good by the F and the E, compared with the A, for the cases of March 1965, January 1977, and 16 January, 1979. On the other hand, the prediction of K_{SE} for the case of 1 January, 1979, is poor. In this case, the magnitude of K_{TE} is extraordinarily large, reflecting the evolution of synoptic situation, that is, blocking ridges were switched from the Pacific to the Atlantic at the middle of the period.
- The transient kinetic energy, K_{TE} is appreciably underestimated by all models. This tendency is particularly pronounced in the

southern hemisphere. The magnitudes of KTE are, in the descending order, the observation, the A, the E, and the F for all cases; the F-model produces the lowest amount of transient eddies.

o Perhaps it is important to restress that the stationary eddies are better simulated, in the descending order, by the F, the E and the A-physics, whereas the transient eddies are not handled well by the elaborate physics. It is, however, not proper at this stage to ascribe the deficient performance to the SGS physics, as will be discussed later.

5.3 The conversion from the potential to the kinetic energy

Figure 22 shows the latitudinal distribution of term, $[-\widehat{\omega^*\alpha^*}]$, which indicates the conversion rate from the eddy available potential energy, A_E to the eddy kinetic energy, K_E, $[\widehat{\ }]$ being the average with respect to the longitude λ and the vertical coordinate σ (the mass weighted vertical average).

Two outstanding points may be noticed.

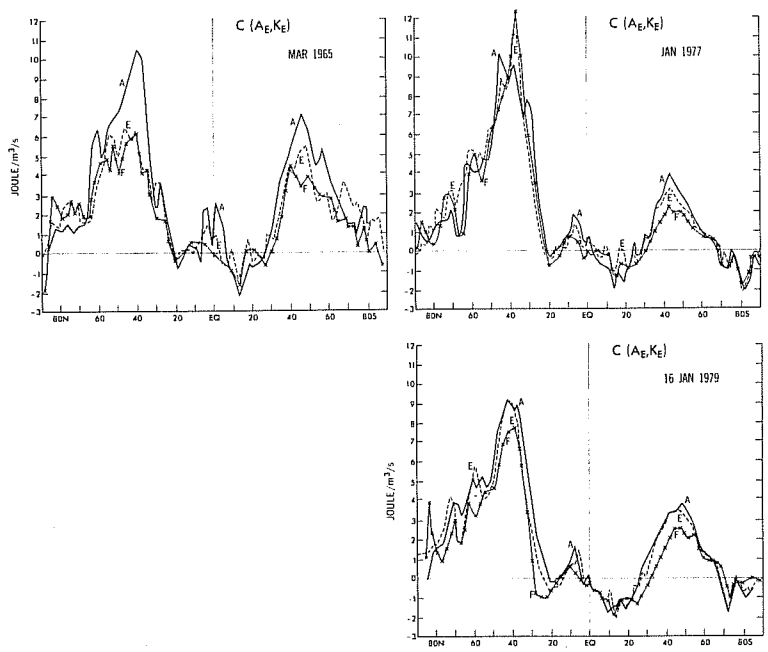

Fig. 22. Latitudinal distributions of the rate of energy conversion from the eddy potential to the eddy kinetic energies, $C(A_E, K_E)$. The case, c, of January 1979 is missing.

o There are three peaks in latitudes. The two large peaks are located at mid-latitudes, and a small one is at 10°N in January cases, and near the equator in March case.

o In both hemispheres, the intensity of $[-\widehat{\omega^*\alpha^*}]$ is, in the descending order, the A, the E, and the F.

The fact that the penetrative convection scheme leads to smaller magnitude of $[-\widehat{\omega^*\alpha^*}]$, and accordingly, to weaker eddy kinetic energy, compared with the Manabe scheme, was also pointed out by Baker et al. (1977; 1978), though their case shows somewhat excessive tendency.

The conversion rates in figure 22 correspond well to the peaks of the transient eddy kinetic energy, K_{TE}, in figure 20 (not K_{SE}) in terms of latitudinal positions. It is plausible to consider that the baroclinic instability is in a close relation with K_{TE} rather than the total eddy kinetic energy (Hayashi and Golder, 1981). These transient eddies are the disturbances generated along the cyclone tracks particularly over oceans.

There is another interesting point. The tropical peak of $[-\widehat{\omega^*\alpha^*}]$ at about 10°N in January corresponds to the peak of K_{TE} in figure 20 for the A and the E. This is almost missing in the F and the observation (NMC). (See also Oort and Peixoto, 1983)

In summary, the elaborate physics generate less transient eddies, because of larger static stability, slower manifold of cloud mass flux, more moderate land surface temperature, more efficient boundary layer physics, and perhaps more effective vertical diffusion in the entire atmosphere.

6. THE PRECIPITATION

6.1 The global distribution

The 30 day mean precipitation distributions for the average of two cases, i.e., 1 January 1977 and 16 January 1979, are displayed in Figure 23, which are compared with the January climatology (Jaeger, 1978).

The first impression of these distributions may be the striking similarity among the models' simulations. However, a closer look may reveal a slight superiority of the F-model over the others. The pronounced feature is that the rainfall distribution in the model is spatially smooth, and is concentrated, in an organized fashion in the oceanic ITCZ (Inter-tropical Convergence Zone) and in the certain areas of tropical continents. On the other hand, the E and the A models produced spatially noisy patterns. The noisiness is more pronounced in the individual case (not shown here). The similar results were obtained by the UK Met. Office experiment (see figures 38 and 39 of Rowntree and Cattle, 1983).

The ITCZ in the Indian ocean is clearly discernible in both hemisphere away from the equator in the F and E models but not in the A model. It is likely that the rainfall over the Indian Ocean is sensitive to the boundary

Fig. 23. Global distributions of the rate of precipitation. January climatology (upper left), the prediction by the A (upper right), the E (lower left), and the F (lower right) in units of cm.s-1. The predictions are the average of two cases, i.e., 1 January 1977 and 16 January 1979, each for monthly average. The contours are: 1.5, 1.0, .5, .2, .1, .05 and 0 cm.s-1. The regions in which the rainfall is larger than .5 cm.s-1 are shaded.

layer parameterization. Namely the Monin-Obukhov similarity process appears to be capable of sensing delicately the ocean temperature.

6.2 The latitudinal distribution

Figures 24 and 25 are the latitudinal distribution of rainfall over land and ocean separately, the rate of rainfall being 30 day means for one March case and three January cases. The climatological values are the March norm and the January norm respectively.

The following may be noted in these figures. (a) The tropical rain is larger over land than over ocean, whereas the mid/high-latitude rain in the Northern hemisphere is larger over ocean than over land. This aspect agrees between the climatology and the models simulation. (b) In all cases, the

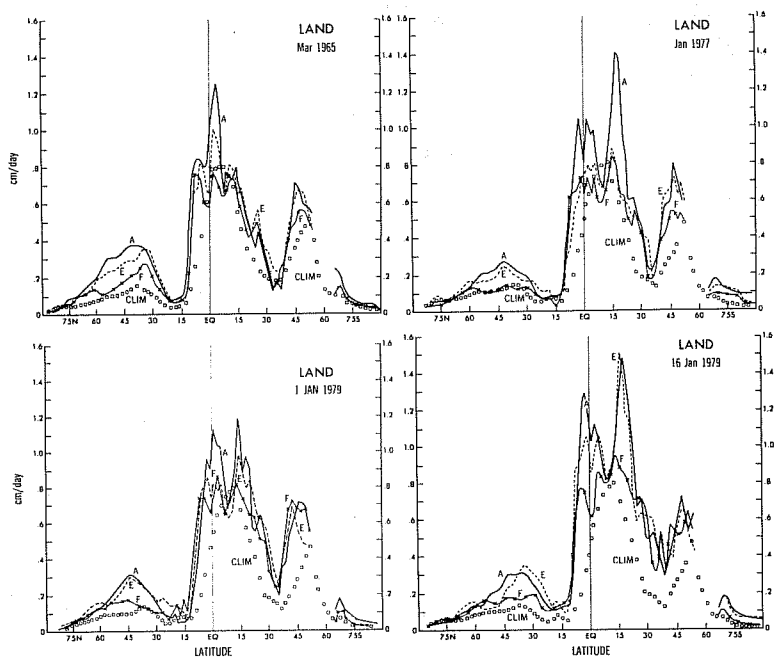

Fig. 24. Latitudinal distributions of the monthly mean rate of precipitation, which is zonally averaged only over land, for four cases (a, b, c, d). The observations are the climatology (small circles); the A (solid lines), the E (dashed lines), and the F (thin solid lines, connecting crosses).

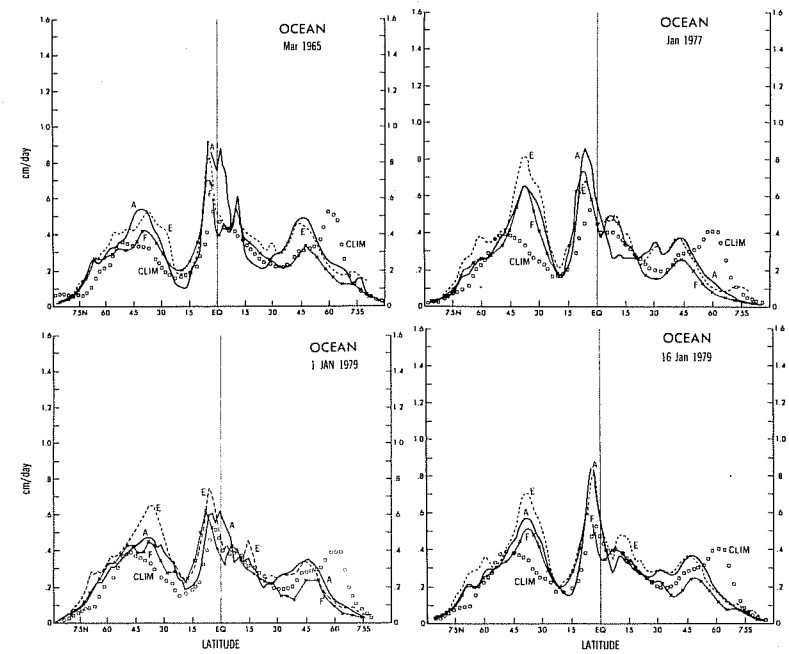

Fig. 25. The same as figure 24 but over ocean.

model's rainfall is substantially or somewhat larger than the climatology. The rates of tropical rainfall in the models are, in the increasing order, in the F, the E and the A-physics. The rate of the mid/high-latitude rainfall is lowest in the F-model; yet it is still larger than the climatology. (c) Over the ocean in the southern hemisphere, the Jaeger's distribution has a maximum at 60°S, whereas the model's rainfall has a maximum at different latitude, i.e., 45°S. Although the Jaeger's maximum is controversial, the models' rain is even more questionable, since the zonal wind in the models, for example, are also shifted equatorward compared with the observation.

It is perhaps generally accepted that the SGS processes manifest their effects in a most dramatic way in the rate of precipitation. Our results agree with this perception. In the tropics, the magnitude of rainfall decreases, in the descending order, in the A, the E, the F and the observation.

One may argue that the excessive rates in the A and the E would be due to the 80%, instead of 100%, condensation criterion. However, as was shown in Miyakoda and Sirutis (1977), in which 100% criterion was used in all three models, the tropical rainfall in the A was still considerably larger than those in the E and the F. Furthermore, the 80% saturation criterion is a part of cumulus parameterization scheme, which is not unreasonable.

In summary, from the standpoint of precipitation rates, the F is best, and the E is next, both over land and ocean and both in the tropics and the mid-latitudes. As has been alluded earlier, the reasonable magnitude of rainfall in the F is ascribed to the slow manifold of cloud mass flux and the large static stability.

The E-physics also contributes to the decrease of precipitation. It is certain that the land-sea contrast of surface physics causes the difference in the A and the E. There was an experiment with a modified A model which has the same physics as the A but uses the homogeneous surface drag coefficient over land and sea. This model has a very sharp peak of rainfall at the equator. This implies that the differential surface drag in the A is effective to push the condensation area from land to sea, where the sea surface temperature controls the condensation, keeping the rain away from the equator.

Coming back to Figures 24 and 25, it may be seen that the rainfall of the E is less than that of the A over land, and that it is not quite so over ocean, and even opposite in the middle latitudes. The reason over land would be the soil heat conduction and possibly the stability-dependent surface boundary layer turbulent processes in the E in contrast to the A. The rainfall over ocean is larger in the E than in the A, over the Indonesian archipelago and north Pacific and north Atlantic. The reason has not been studied yet.

The quality of the rainfall in the three models will be discussed in the next subsection.

6.3 The GATE study

Figure 26 is the geographical distribution of precipitation rates over the GATE (GARP Atlantic Tropical Experiment) A-area, obtained by the forecasts of the E and the F models, and by the observation based on the infrared imagery taken by the SMS-1 satellite (Woodley et al., 1975; 1980). The forecasts were started at 00GMT 24 August, 1974, using the four-dimensional analysis (Miyakoda et al., 1982) based on an augmented GATE data set, and the integrations were carried out for one-month period. However, Figure 26 shows the 28 day average of the rainfall, since the infrared observation is available only for that period.

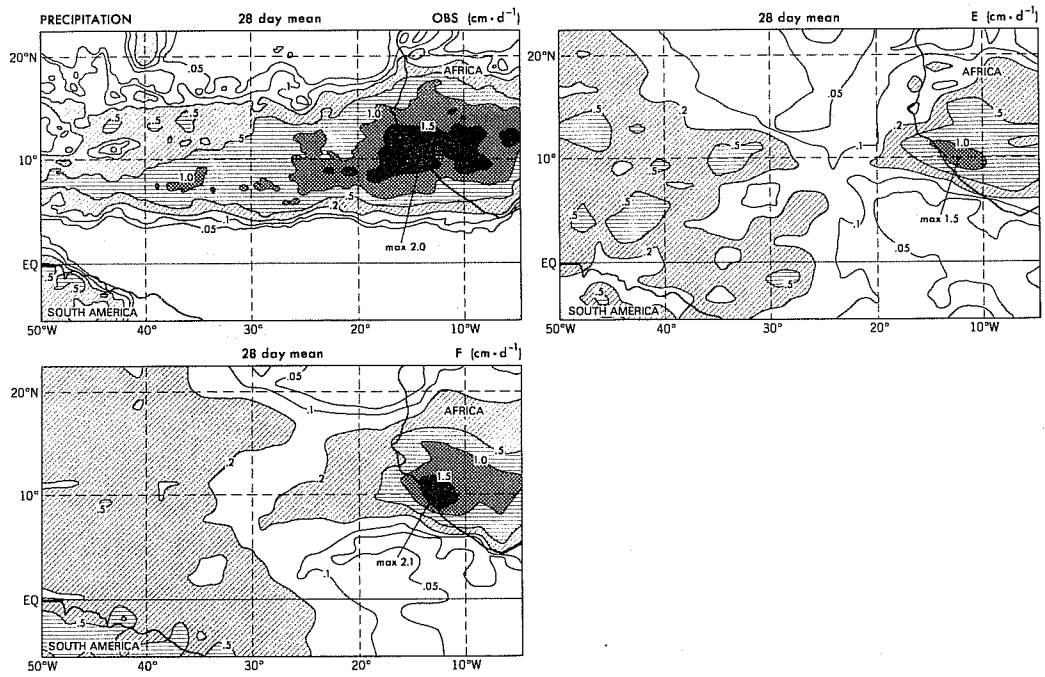

Fig. 26. Predicted rates of precipitation for 28 days, starting on 24 August, 1974, over the GATE A-scale area, in Atlantic and western Africa. The observation based on satellite infrared measurement (upper left), the E (upper right), and the F (lower left).

The moist convective adjustment produced the precipitation that is scattered in a wide domain as in the upper right, whereas the F-model generated the reasonable distribution as in the lower left. These precipitations are associated with African easterly waves, which start in the central Africa and propagate westward. The intensity of rainfall reaches maximum before the waves leave African coasts, and yet the decay is slow over the ocean. In this respect, the forecast rainfall decays more rapidly, the reason being unclear.

7. SIGNIFICANCE OF THE SGS PARAMETERIZATIONS

The SGS parameterizations involved in the E beyond those of the A are "dry turbulent processes". These SGS processes are the logical outcome from the discretization of the model's atmosphere. The formulas are derived in a straightforward way by applying the running means of a grid length to the equations of motion and thermodynamics and utilizing turbulent theories and observational data. There would be not much room to suspect whether these parameterizations are unnecessary and unreasonable, though it may be argued whether the effects are properly included in GCMs (see Manton, in this workshop report) and whether the Rotta and the Kolmogoroff assumptions are adequate.

On the other hand, the cumulus parameterization is more heuristic, more hypothetical, and more complex. A question often raised is whether it is really necessary or useful.

7.1 The parameterization of penetrative convection

Yamasaki (1977) and Rosenthal (1977) attempted successfully to make hurricane simulation without any cumulus parameterization. Orlanski and Ross (1984) demonstrated that the squall lines can be reproduced numerically with the so-called explicit convection.

A similar situation exists for the numerical simulation of the general circulation. A test of one-month integration was conducted without any cumulus parameterization. The GCM includes the E-physics but excludes the moist convective adjustment (let us denote it "G-physics). In this case, gigantic cumuli of grid-size were generated and yet the GCM integration proceeded without any numerical trouble.

The predicted pattern of 500 mb geopotential height on Day 10 for the case of January 1977 turned out to be surprisingly good (not shown here). Other variables are also reasonable and are as good as those in other models such as the E-model. The only problem is that the rain distribution is not reasonable. Figure 27 is the space distribution of 10 day mean rate of rainfall along a zonal rainbelt at the tropical latitude of 9.35°S. The rain in the G has spikes, which are associated with the huge cumulonimbi. This tendency is also seen in the rain of the E-model but to lesser extent. The precipitation of the F has broader distribution pattern.

Comparing the predicted geopotential height patterns by the G, the E and the F-models, it is revealed that the pattern of the G-model maintains the vortex over the north America, as is found in the observation, whereas the map of the F-model missed this vortex entirely. It is unclear whether the upper layer heating or the momentum transport due to the cumulus convection in

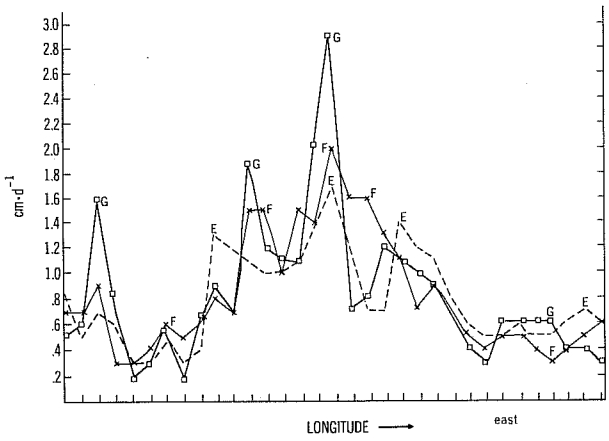

Fig. 27. An example of spatial distributions of predicted rainfall by the G (solid lines connecting squares), the E (dashed lines), and the F (solid lines connecting crosses) in units of cm/day.

the F-model caused the adversary effect to the stratospheric vortex. The gravity wave generation is, however, largest in the G, next in the E, and smallest in the F. The skill score shows that the G's result is slightly poorer than the E's for the 30 day time range (not shown here).

This indicates that there is some advantage in utilizing cumulus parameterization, though the merit is subtle for the simulation of the general circulation but substantial for that of the precipitation. There are two additional evidences: one is the tropical rainfall study, and the other is the experience of the short-term weather forecast.

Lord (1979) applied Arakawa-Schubert parameterization to estimate of precipitation over a small tropical region in GATE in a semi-prognostic framework, and demonstrated an excellent agreement with the observed time variation of rainfall, while the agreement of the estimate with other schemes were not quite good. Thus the F-model may provide not only the reasonable geographical distribution of precipitation, but also have a potential to provide quantitatively accurate rainfalls associated with individual tropical waves. Krishnamurti et al. (1980) showed that the Kuo parameterization is equally good as the Arakawa-Schubert scheme.

Hammarstrand (1977) and other investigators studied the quality of rainfall estimate in short-range forecasts (one or two days) at the mid- and high-latitudes, and concluded that the Kuo scheme gave better forecasts than the Manabe scheme. More recently, Leslie (1981) has compared the cumulus parameterization schemes, based on 61 case studies, and assessed that the Arakawa-Schubert scheme and the recent Kuo schemes are greatly superior to the Manabe scheme in the intensity and distribution of the predicted rainfall patterns. (See also the result of Golding in this workshop.)

If this is true, it may be summarized that the penetrative cumulus parameterization provides some significance and advantage in forecasting precipitation. (The issue is still controversial. There is a report that with a fine grid model the explicit convection is superior to a parameterization - Orlanski, private communication.)

7.2 The calculation of ratio

In order to assess the significant response to various SGS physics, a ratio was calculated based on the formula

$$r = [\widehat{|\Delta|}] \,/\, [\widehat{\sigma(\chi)}] \,, \qquad (7.1)$$

where $\sigma(\chi)$ is the standard deviation of a variable χ, Δ is the difference of χ between two physics, for example, χ is the 20 day mean for Day 10-30, and $[\widehat{\ }]$ denotes the zonal and vertical average. The denominators are estimated by the standard deviation,

$$\sigma^2(\chi) = \sum_{i=1}^{n} (\chi_i - \langle\chi\rangle)^2/n \qquad (7.2)$$

where $\langle\chi\rangle$ is the ensemble mean with respect to the sample number n.

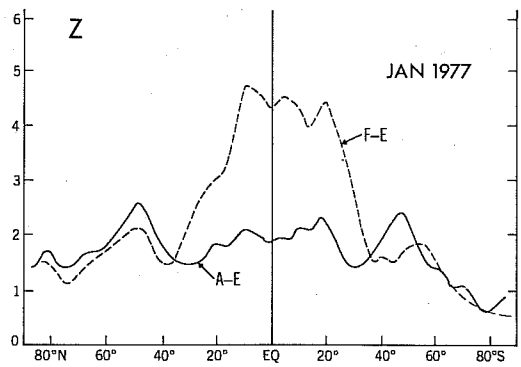

Fig. 28a. Latitudinal distribution of the ratio for the geopotential height differences between the F and the E, and between the A and the E, for the case of January 1977.

Three monthly predictions were generated from three different initial conditions for each sample case, using the E-model (see Miyakoda et al., 1983). The signal levels are estimated by the difference Δ as

$$\Delta = \chi_F - \chi_E \tag{7.3}$$

or

$$\Delta = \chi_A - \chi_E \tag{7.4}$$

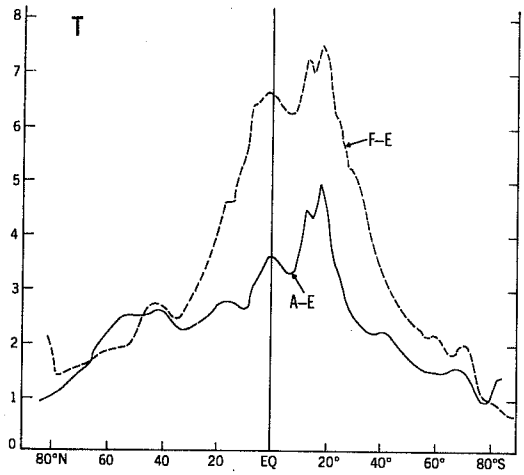

Fig. 28b. The same as figure 28a, but for the temperature.

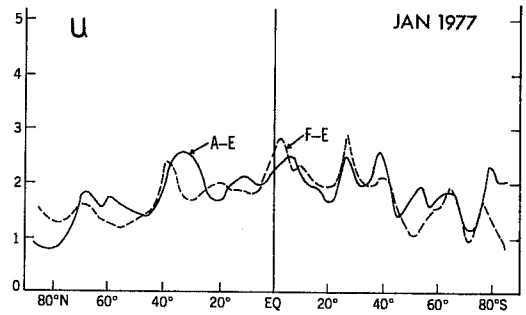

Fig. 28c. The same as figure 28a, but for the zonal wind.

Thus, the ratio r indicates the response of the A or the F physics relative to the E physics. In general, if r>1, the difference is assumed to be appreciable. Chervin and Schneider (1976 b) and Hayashi (1982) have proposed estimates of the signal-to-noise ratio. However, Eq. (7.1) is different from those definitions. Hayashi (personal communication) mentioned that Eq. (7.2) is quite different from that in the definition of signal-to-noise ratio, and besides, the sample number in our case is extremely small.

Figure 28 shows the latitudinal distributions of the ratio in the case of 1 January, 1977, for the geopotential height z, the temperature T, the wind components u and v. The similar results were obtained for the case of 16 January, 1979. Thus figure 28 together with the result of 1979 lead to the following conclusions.

- The largest ratios are noted in the differences of the geopotential height z and the temperature T between the F and the E in the tropics.
- The ratio of the temperature T between the A and the E in the tropics is also large but to lesser extent.
- The ratio for u or v is not quite large as that of T or z. Yet there is a tendency that the ratio in the tropics is appreciably larger than in the extratropics.

Figure 29 is the vertical distribution of the ratio for T at the equator, i.e.,

$$r' = [|\Delta|] \,/\, [\sigma(\chi)] \qquad (7.5)$$

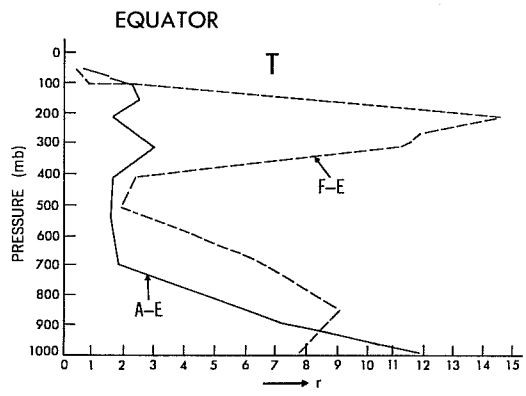

Fig. 29. Vertical distribution of signal-to-noise ratio for the temperature differences between the F and the E, and between the A and the E, for the case of January 1977.

The response of the F-physics is really large in the layer between 400 and 100 mb level; r' is about 9. This effect is generated solely by the cumulus convection. The difference between A and E models is also appreciable in the lower atmosphere, implying that the boundary layer physics caused a considerable effect in the tropics. The similar effect is also noticed in the vertical distribution of r' for u at the equator (not shown here). Attention is called for the fact that the ratio for the geopotential height z is above a unity for most of the latitudes except high latitudes.

8. REMARKS

8.1 The mechanism of impacts

Figures 28 and 29 indicate that the impact is significant in the tropics. In other words, the effects of SGS parameterization expressed by the A, the E, and the F models have been detected unerringly in the tropical temperature and pressure, and probably precipitation, whereas the effects for the extratropics have not yet been proved. Only evidence for the extratropics is the skill scores for the 10 day mean geopotential height maps in figures 2, 3 and 4, though a great caution should be exerted on attaching the statistical validity to the conclusions based on only four cases.

Let us, at the moment, assume that this is true. Then a question may arise as to why and how the stationary or the slowly varying eddies can be

better predicted by the E and the F than the A. The advantage of the E-physics over the A is particularly noticed in connection with blocking episodes. Since the mechanism of blocking has not been fully understood, it is not easy to discuss this matter.

There are, at least, two schools of thoughts on the mechanistic accounts of blocking (for example, Kinter, 1983). The first postulate is that a solitary blocking ridge at high latitudes develops if local zonal westerlies upstream of the key geographical region are appropriate (generally weaker than normal), in conjunction with mountain effect. The second postulate is that baroclinic transient eddies interact with pre-existing downstream stationary waves to generate a resonance-like amplification (for example, Kalnay and Merkin, 1981; Dole, 1981).

In section 4, the substantial impact of the SGS physics on the sector mean of zonal wind was mentioned. The meridional profile of the zonal wind in figure 18 may be suggestive of the clues for the link between the SGS parameterizations and the overall GCMs' performance in the skill score. The SGS parameterizations appear to be critical in producing adequate meridional profiles of local zonal wind, which, in turn, determine the appropriate positive index anomalies.

There are four major changes in the SGS processes from the A to the E. They are: the removal of dry convective adjustment, the improved transfer physics at the Earth's surface, the soil heat conduction, and the vertical diffusion of momentum and heat above the planetary boundary layer. The second and third factors improve the effect of land-sea contrast, and, therefore, the Earth's surface conditions are better included in the solution of the GCM. The removal of dry convective adjustment could be attributable to the simulating capability of the zonal flow at high latitudes. However, our efforts of tracing the causes stop at this point. The further investigation is a future work.

The differences in the GCM performance between the F and the E are substantial. There are two major changes in the cumulus parameterization from the E to the F, i.e., the larger heating in the upper level and inclusion of vertical momentum transport. The former leads to more stable stratification in the upper layer. Dynamic theory predicts that the static stability is extremely important for determining the non-zonal kinetic energy and the eddy meridional heat transport (Held, 1978).

In the F-model, the conversion of potential to kinetic eddies is reduced, and the magnitudes of transient eddies are decreased, while the magnitudes of stationary eddies remain intact, and the longitudinal phase of stationary eddies are improved. The F simulates the condensation associated with extratropical cyclones better than the E, and the quality of cyclone-scale forecast affect the simulation of ultra-long waves.

Because of stabler stratification and the method used to obtain the cloud mass flux, the F generates less gravity waves, particularly in the tropics, than the E, and other small scale variability tends to be suppressed in the F. It is not known, however, whether these effects are beneficial for prediction.

With regards to the tropics, a large number of investigations have recently been conducted on the teleconnection effect of tropical sea surface temperature anomalies on the mid-and the high-latitudes. In particular, persuasive theories (Hoskins and Karoly, 1981; Simmons, 1982) and convincing observational evidences (Horel and Wallace, 1982; Rasmusson and Carpenter, 1982) have been offered. If one looks at the magnitude of precipitation differences among the A, the E, and the F in figures 23 and 26, the magnitude is as much as 0.5 cm/day locally (in Indonesian Archipelago), 0.2 cm/day in the zonal average over ocean, and 2.0 cm/day in the zonal average over land. These amounts are comparable to the increment of precipitation in tropics due to the sea surface temperature anomalies in the case of El Nino.

The SGS parameterization is the matter of improvement of quality on the internal dynamical process in GCM's, whereas the sea surface temperature anomalies are the matter of imposition of external forcing as the boundary condition for the GCMs integration. The slowly varying boundary effects in tropics have a potential to increase the predictability of time-averaged circulation in mid-latitudes, and besides, the tropical flows may be potentially more predictable than those in mid-latitudes (Shukla, 1982). It may be appropriate, therefore, to rectify first the internal dynamics of GCM, and thereafter, to prescribe correct anomalies of external forcings.

8.2 The space resolution

As was mentioned earlier, the A and the E-physics of N48L18 models were applied to the 30 day integrations, using the initial condition of 00GMT, 1 March, 1965. Figures 30 and 31 are the vertical and the latitudinal

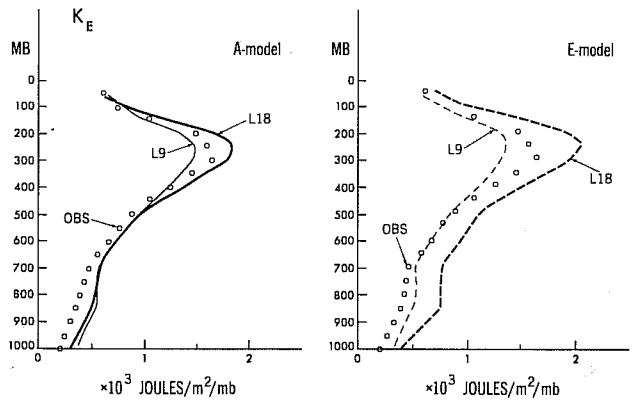

Fig. 30. Vertical distributions of eddy kinetic energy by the L9 (nine level) and the L18 models, compared with the observation (small circles). The A (left) and the E (right).

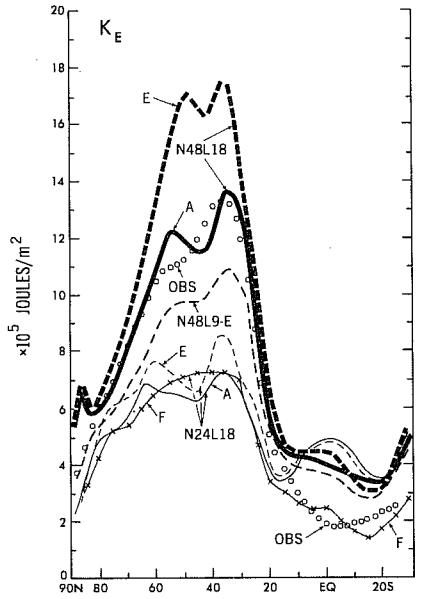

Fig. 31. Latitudinal distributions of eddy kinetic energies by various models, averaged zonally, vertically and over a month of March, 1965. The observation (small circles), the A, the E and the F of N24L18 (thin lines), the E of N48L9 (thicker dashed line), and the A and the F of N48L18 (thick lines).

distribution of K_E, respectively, obtained by the L18 and the L9 models. In figure 31, the N24L18 models are also included. These figures indicate that the eddy kinetic energy increases with the vertical resolution. It is interesting to note that the transient eddies, i.e., K_{TE} is enhanced, though K_{SE} is also to some extent increased in the L18 model. This characteristic is confirmed by an independent study, using spectral models of L9 and L18.

It appears that to achieve an appropriate intensity of K_{TE} in a GCM is an extremely challenging task. For example, in the study of space resolution impact in GCM's, Manabe et al. (1979) obtained a result that the increase of lateral space resolution of a GCM leads to more stationary eddies and, yet, unfortunately, less transient eddies.

From the experiences gained so far, it is speculated that, in order to obtain reasonable magnitude of K_{SE} and K_{TE} and their partition, a high space resolution of the GCM in both vertical and horizontal is required. Besides an adequate aspect ratio between the vertical and the lateral resolution has to be considered together with an appropriate SGS diffusion for vertical and lateral, pertinent to the specific spatial resolution. In addition, the advanced SGS physics and the cloud-interaction should be properly included (see Tiedke, 1983). Cloud-interaction and prescription of sea-surface temperature anomalies increase the transient eddies.

9. CONCLUSIONS

Tentative conclusions based on four samples are as follows.

(i) The F- and E-models showed better performance in the medium-range forecasts of about 10 days, compared with the A-model. The effects are subtle yet substantial.

(ii) The superiority of the F over the E- and A-models is more evident for the 30 day integrations.

(iii) The stationary azonal eddies are best simulated by the F, and next by the E-model.

(iv) The geographical distribution of rainfall in the F-model appears better than in other models. The predicted distribution agrees well with the observation in GATE, for example.

The precipitation pattern in the F emerges in an organized fashion rather than in a scattered pattern, and the rainfall distributes more gradually and smoothly than in other models.

The precipitation pattern in the E-model is better than in the A. The improved rainfall over ocean is probably due to the refined surface physics, and the moderate rainfall over land is presumably due to the soil heat conduction.

(v) It is a most pronounced result that the squared vertical velocity, ω^2, is substantially smaller in the F than in other models, corresponding to less gravity noise and less tropical precipitation. The E gives slightly less ω^2 than the A.

(vi) Another pronounced result is that vertical thermal stratification is most stable in the F. This is the direct consequence of the penetrative convection in the F.

(vii) In the experiment of the N48L9 models, the magnitude of the transient eddy kinetic energy is, in the decreasing order, the A, the E and the F-models, particularly in the southern hemisphere but, to lesser extent, in the northern hemisphere as well. This is another consequence of the penetrative convection scheme. The magnitude of $[-\overline{\omega'\alpha'}^{\sigma}]$ and ω^2 also decrease appreciably in the F compared with other physics.

(viii) The hemispheric integral of the azonal eddy kinetic energy is overwhelmingly affected by the model's space resolution in this resolution range.

(ix) The zonally averaged zonal winds in the upper atmosphere in the F-model are somewhat large in the extratropics.

(x) The zonally averaged zonal winds at high latitude, say 35°-65°N, tend to be larger in all of the models than the observed.

(xi) The method to use the lifting condensation as the cloud base in the Arakawa-Schubert cumulus parameterization appears to work satisfactorily.

(xii) The difference of the geopotential height and the temperature between the F and the E-physics is significantly large in the tropics. The difference between the A and the E is also appreciable in the tropics, but to lesser extent.

Acknowledgements.

Gratiutde is expressed to Professor A. Arakawa and Dr. S. Lord, who provided us with the programs of the Arakawa-Schubert method. The authors wish to acknowledge for the reviews of Drs. Y. Hayashi, I. Orlanski, Y. Kurihara, S. Manabe and T. Gordon. The authors' thanks also go to P. Tunison, J. Pege and J. Conner for their careful and enthusiastic assistance.

APPENDIX I

Mixed Layer Depth

Using the N24L18 model and March 1965 data, the mixed layer depths obtained by various models were investigated. Figure A-1 is an example of these results. This indicates the depths from the F2-physics which uses Randall's scheme (Randall, 1976), and the F3-physics which used the lifting condensation level (LCL). As additional information, the LCL in the F2-model is shown. The condensation criterion is 100% for both models.

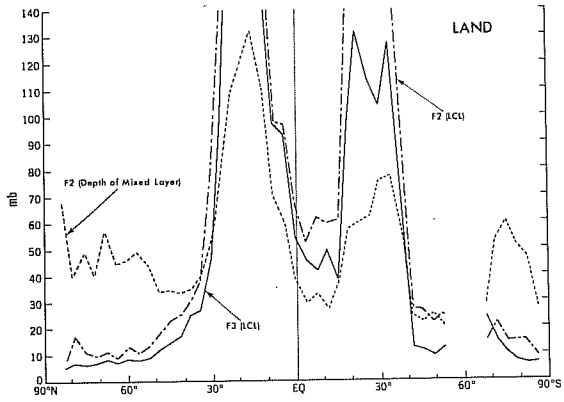

Fig. A1a. Latitudinal distributions of the LCL (lifting condensation level) of the F2 and the F3-models, and the depth of mixed layer of the F2, over land.

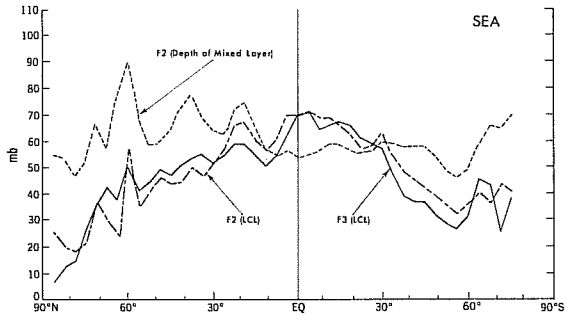

Fig. A1b. The same as figure A1a, but over sea.

The LCL over land is much larger than the mixed layer depth in the F2 model, whereas both levels are comparable over the tropical ocean. The depth estimated by Randall's scheme is substantially larger at high latitudes. (Note that the recent Randall's model gives lower height, Randall, 1982).

APPENDIX II

The meridional profile of zonal wind at high latitudes may be detrimental for determining meandering patterns of downstream westerlies. The intensities of zonal wind north of say 40°N are statistically weaker in the positive index pattern than in the negative index pattern of the teleconnection of Wallace and Gutzler (1981). Figure A2 is the observed profile of sector mean of zonal wind for Pacific-North-American (PNA) patterns based on the 15 year data (Kinter, 1984). The vertical bars in the figure indicate the range of variability among the 15 year data. The similar feature in the sector mean of

zonal wind can be obtained for the West Atlantic (WA) pattern. The possibility of the weak zonal wind in high latitudes for the case of the blocking actions was also suggested previously (Miyakoda et al., 1983) with respect to the case of January 1977.

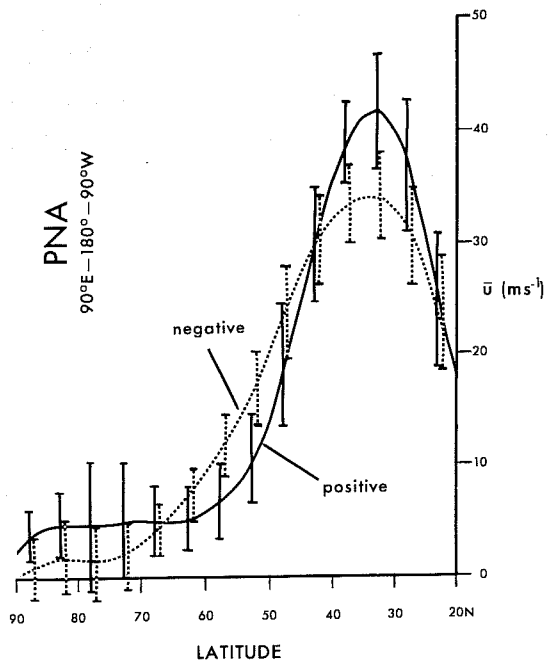

Fig. A2. The zonal wind at 300 mb as a function of latitude for the positive and negative PNA index cases (after Kinter, 1983).

REFERENCES

Arakawa, A. and Schubert, W. H. 1974 Interaction of cumulus cloud ensemble with the large-scale environment, Part I. J. Atmos. Sci., 31, 674-701.

Baker, W.E., Kung, E.C. and Somerville, R.C.J. 1977 Energetics diagnostics of the NCAR general circulation model. Mon. Wea. Rev., 105, 1384-1401.

Baker, W.E., Kung, E.C. and Somerville, R.C.J. 1978 An energetics analysis of forecast experiments with the NCAR general circulation model. Mon. Wea. Rev., 106, 311-323.

Bengtsson, L. 1981 Numerical prediction of atmospheric blocking - a case study. Tellus, 33, 19-42.

Carson, D.J. and Richards, P.J.R. 1978 Modelling surface turbulent fluxes in stable conditions. Bound. Layer Meteor., 14, 67-81.

Chervin, R.M. and Schneider, S.H. 1976a A study of the response of NCAR GCM climatological statistics to random perturbations: Estimating noise levels. J. Atmos. Sci., 33, 391-404.

Chervin, R.M. and Schneider, S.H. 1976b On determining the statistical significance of climate experiments with general circulation models. J. Atmos. Sci., 33, 405-412.

Clarke, R.H. 1970 Recommended methods for the treatment of the boundary layer in numerical models. Australilan Meteorol. Mag., 18, 51-73.

Dole, R.M. 1981 Persistent anomalies of the extratropical Northern Hemisphere wintertime circulation.

Donner,L.J., Kuo, H-L and Pitcher, E.J. 1982 The significance of thermodynamic forcing by cumulus convection in a general circulation model. J. Atmos. Sci., 39, 2159-2181.

Hammarstrand, U. 1977 On parameterization of convection for large scale numerical forecasts at mid-latitudes. Beitr. Phys. Atmos., 50, 78-88.

Hayashi, Y. 1982 Confidence intervals of a climate signal. J. Atmos. Sci., 39, 1895-1905.

Hayashi, Y. and Golder, D.G. 1981 The effects of condensational heating on midlatitude transient waves in their mature stage: control experiments with a GFDL general circulation model. J. Atmos. Sci., 38, 2532-2539.

Held, I.M. 1978 The tropospheric lapse rate and climate sensitivity: Experiments with a two-level atmospheric model. J. Atmos. Sci., 35, 2083 - 2098.

Held, I.M. 1982 Stationary and quasi-stationary eddies in the extra-tropical troposphere: theory. Academic Press, B. Hoskins (ed), 127-168.

Helfand, H.M. 1979 The effect of cumulus friction on the simulation of the January Hadley circulation by the GLAS model of the general circulation. J. Atmos. Sci., 36, 1827-1843.

Hicks, B.B. 1976 Wind profile relationships from the "Wangara" Experiment. Quart. J. Roy. Meteor. Soc., 102, 535-551.

Hollingsworth, A., Arpe, K., Tiedtke, M, Capaldo, M. and Savijärvi, H. 1980 The performance of a medium-range forecast model in winter-impact of physical parameterization. Mon. Wea. Rev., 108, 1736-1773.

Holton, J.R. and Colton, D.E. 1972 A diagnostic study of the vorticity balance at 200 mb in the tropics in the northern summer. J. Atmos. Sci., 29, 1124-1128.

Horel, J.D. and Wallace, J.M. 1981 Planetary-scale atmospheric phenomena associated with the interannual variability of sea surface temperature in the equatorial Pacific. Mon. Wea. Rev., 109, 813-829.

Hoskins, B.J. and Karoly, D.J. 1981 The steady linear response of a spherical atmosphere to thermal and orographic forcing. J. Atmos. Sci., 38, 1179-1196.

Jaeger, L. 1978 Monatskarten des Niederschlags für die ganze Erde. Berich. Dtsch. Wetterdienst., 18, No. 139, 38pp.

Kalnay-Rivas, E. and Merkine, L.O. 1981 A simple mechanism for blocking. J. Atmos. Sci., 38, 2077-2091.

Kinter, J.L. and Miyakoda, K. 1983 A numerical study of planetary scale waves and blocking patterns using barotropic models. Research Activities in Atmospheric and Oceanic Modeling. Numerical Experimentation Programme, World Climate Research Programme. Report No. 5, (ed.) I. D. Rutherford, 3.4-3.7.

Kinter, J.L. 1983 Barotropic studies of stationary extratropical anomalies in the troposphere. Ph.D. thesis, Geophysical Fluid Dynamics Program, Princeton University.

Kuo, H-L. 1965 On formation and intensification of tropical cyclones through latent heat release by cumulus convection. J. Atmos. Sci., 22, 40-63.

Kuo, H-L. 1974 Further studies of the parameterization of the influence of cumulus convection on large-scale flow. J. Atmos. Sci., 31, 1232-1240.

Krishnamurti, T.N., Ramanathan, Y., Pan, Hua-Lu, Pasch, R.J. and Molinari, J. 1980 Cumulus parameterization and rainfall rates I. Mon. Wea. Rev., 108, 465-472.

Kurihara, Y. and Holloway, J.L. Jr. 1967 Numerical integration of a nine-level global primitive equations model formulated by the box method. Mon. Wea. Rev., 95, 509-530.

Leslie, L.M. 1981 Comparative performance of convective parameterization schemes in a short-term prognosis model. Contrib. to Atmos. Phys., 54, 173-185.

Lord, S.J. 1978 Development and observational verification of a cumulus cloud parameterization. Ph.D. thesis, University of California at Los Angeles, 359 pp.

Lord, S.J. 1979 Verifications of cumulus parameterization using GATE data. Proceedings of the Seminar on the Impact of GATE in Large-Scale Numerical Modeling of the Atmosphere and Ocean. Woods Hole, Mass., August 20-29, 1979, GATE Panel, The National Research Council, 182-191.

Lord, S.J., Chao, W.C. and Arakawa 1982 Interaction of a cumulus cloud ensemble with the large scale environment. Part IV. The discrete model. J. Atmos. Sci., 39, 104-113.

Lyne, W.H. and P.R. Rowntree 1976 Development of a convective parameterization using GATE data. Met. O. 20, Technical Note II/70, Meteorological Office, Bracknell.

Manabe, S., Smagorinsky, J. and Strickler, R.F. 1965 Simulated climatology of a general circulation model with a hydrological cycle. Mon. Wea. Rev., 93, 769-798.

Manabe, S., Hahn, D.G. and Holloway, J.L. 1979 Climate simulations with GFDL spectral models of the atmosphere: Effect of spectral truncation. Report of the JOC Study Conference on Climate Models: Performance, intercomparison and sensitivity studies at Washington, D.C., 3-7 April, 1978. GARP Publication Series No. 22, W. L. Gates (ed.), 41-94

Mellor, G.L. and Yamada, T. 1974 A hierarchy of turbulent closure models for planetary boundary layers. J. Atmos. Sci., 31, 1791-1806.

Mellor, G.L. and Yamada, T. 1977 A turbulence model applied to geophysical fluid problems. Proceedings of a symposium on Turbulence Shear Flows, April 18-20, Penn. State Univ., Pa.

Miyakoda, K. and Sirutis, J. 1977 Comparative global prediction experiments on parameterized subgrid-scale vertical eddy transports. Beitr. z Phys. d Atmos., 50, 445-487.

Miyakoda, K., Sheldon, J. and Sirutis, J. 1982 Four-dimensional analysis experiment during the GATE period Part II. J. Atmos. Sci., 39, 486-506.

Miyakoda, K., Gordon, T., Caverly, R., Stern, W., Sirutis, J. and Bourke, W. 1983 Simulation of a blocking event in January 1977. Mon. Wea. Rev., 111, 846-869.

Oort, A.H. and Peixoto, J.P. 1983 Global angular momentum and energy balance requirements from observations. Advances in Geophysics, 25, 355-490.

Oort, A. 1983 Global atmospheric circulation statistics, 1958-1973. NOAA Professional Paper 14, Rockville, MD, 180 pp.

Orlanski, I. and Ross, B.B. 1984 The evolution of an observed cold front Part II: Mesoscale dynamics. (To appear in J. Atmos. Sci.)

Peixoto, J.P. and Oort, A.H., 1974 The annual distribution of atmospheric energy on a planetary scale. J. Geophys. Res., 79, 2149-2519.

Ploshay, J.J., White, R.K. and Miyakoda, K. 1983 FGGE Level III-B daily global analysis Part I (Dec. 1978 - Feb. 1979). NOAA Data Report, ERL GFDL-1, Geophysical Fluid Dynamics Laboratory, Princeton, N.J., 278 pp.

Randall, D.A. 1982 Performance of the PBL parameterizations in the GLAS and UCLA models. ECMWF Workshop proceedings.

Randall, D.A. 1976 The interaction of the planetary boundary layer with large-scale circulations. Ph.D. Thesis, The University of California, Los Angeles. 247 pp.

Rasmusson, E.M. and Carpenter, T.H. 1982 Variations in tropical sea surface temperature and surface wind fields associated with the Southern Oscillation/El Nino. Mon. Wea. Rev., 110, 354-384.

Rowntree, P.R. and Cattle, H. 1983 The Meteorological Office GATE Modelling Experiment. UK Met. Office, Scientific Paper No. 40 Met. O. 946, 76pp.

Rosenthal, S.L. 1977 Numerical simulation of tropical cyclone development with latent heat release by the resolvable scales. I: Model description and preliminary results. J. Atmos. Sci., 35, 258-271.

Schneider, K.E. and Lindzen, R.S. 1976 A discussion of the parameterization of momentum exchange by cumulus convection. J. Geophys. Res., 81, 31581-3161.

Shukla, J. 1982 Predictability of time averages: the influence of the boundary forcing. NASA Technical Memorandum 85092, Laboratory for Atmospheric Sciences, Global Modeling and Simulation Branch, NASA Goddard Space Flight Center, Greenbelt, Maryland 20771, 34pp.

Simmons, A.J. 1982 The forcing of stationary wave motion by tropical diabatic heating. Quant. J. R. Meteor. Soc., 108, 503-534.

Stone, P.H., Quirk, W.J. and Somerville, R.C.J. 1974 The effect of small-scale vertical mixing of horizontal momentum in a general circulation model. Mon. Wea. Rev., 102, 765-771.

Tiedtke, M., Geleyn, J.F., Hollingsworth, A. and Louis, J-F. 1979 ECMWF model parameterization of sub-grid scale processes. Technical Report, No. 10, European Centre for Medium Range Weather Forecasts, 45 pp.

Tiedtke, M. 1983 Winter and summer simulations with the ECMWF model. Workshop on Intercomparison of Large-scale Models Used for Extended Range Forecasts. 30 June - 2 July, 1982. European Centre for Medium Range Weather Forecasts, 263-313.

Tiedtke, M. 1984 The effect of penetrative cumulus convection on the large-scale flow in a general circulation model. ECMWF Tech. note.

Umscheid, L. and Bannon, P.R. 1977 A comparison of three global grids used in numerical prediction models. Mon. Wea. Rev., 105, 618-635.

Wallace, J.M. and Gutzler, D.S. 1981 Teleconnections in the geopotential height field during the Northern Hemisphere winter. Mon. Wea. Rev., 109, 784-812.

Woodley, W.L., Griffith, C.G., Griffin, J.S. and Stromatt, S.C. 1980 The influence of GATE convective rainfall from SMS-1 imagery. J Appl. Meteor. 19, 388-408.

Woodley, W.L., Olsen, A.R., Herndon, A. and Wiggert, V. 1975 Comparison of gage and radar methods of convective rain measurements. J. Appl. Meteor., 14, 909-928.

Yamada, T., and Mellor, G.L. 1980 A numerical simulation of BOMEX data using a turbulence closure model coupled with ensemble cloud relations. Q. J. Roy. Meteor. Soc., 105, 915-944.

Yamasaki, M. 1977 A preliminary experiment of the tropical cyclone without parameterizing the effects of cumulus convection. J. Meteor. Soc. Japan, 55, 11-30.